Uncertainty quantification for systems of conservation laws

Gaël Poëtte [a,b,*], Bruno Després [a], Didier Lucor [b]

[a] Commissariat à l'Énergie Atomique, Centre DAM, Ile de France, Bruyères le Châtel, 91297 Arpajon Cedex, France
[b] Institut Jean Le Rond D'Alembert Université Pierre et Marie Curie, 4 place Jussieu, 75252 Paris, France

ARTICLE INFO

ABSTRACT

Uncertainty quantification through stochastic spectral methods has been recently applied to several kinds of non-linear stochastic PDEs. In this paper, we introduce a formalism based on kinetic theory to tackle uncertain hyperbolic systems of conservation laws with Polynomial Chaos (PC) methods. The idea is to introduce a new variable, the *entropic variable*, in bijection with our vector of unknowns, which we develop on the polynomial basis: by performing a Galerkin projection, we obtain a deterministic system of conservation laws. We state several properties of this deterministic system in the case of a general uncertain system of conservation laws. We then apply the method to the case of the inviscid Burgers' equation with random initial conditions and we present some preliminary results for the Euler system. We systematically compare results from our new approach to results from the stochastic Galerkin method. In the vicinity of discontinuities, the new method bounds the oscillations due to Gibbs phenomenon to a certain range through the entropy of the system without the use of any adaptative random space discretizations. It is found to be more precise than the stochastic Galerkin method for smooth cases but above all for discontinuous cases.

1. Introduction

High efficiency in the resolution of complex partial differential equations comes along with the need for increasing computer power and memory. In view of the presently achievable accuracy of such simulations, several questions arise: what does this accuracy mean if there exist doubts at some crucial step of the resolution? Can we rely on the chosen initial conditions, boundary conditions and model parameters for the computation of the numerical solution? How is the solution influenced by these unknowns? A tradeoff has to be made between accurate deterministic solutions and treatment of the uncertainties.

Polynomial Chaos (PC) based methods aim at answering those questions. They were first introduced by Ghanem and Spanos [11] and are related to the seminal work of Wiener on the Homogeneous Chaos Theory [42]. They appear to be a good alternative to statistical methods (as Monte–Carlo simulations and its variants) for Uncertainty Quantification (UQ). PC methods were successfully used for solving many problems (stochastic elastic materials [11], finite deformations [2], heat conduction [39], incompressible flows [44,32,27], reacting flows and detonation [23], etc.). PC gives rich statistical information through the polynomial coefficients (moments, Sobol sensitivities, probability density function (pdf), etc.). Two variants that we shall discuss in more details in this work are important in practice: the stochastic collocation implementation (nonintrusive) uses a deterministic code as a black-box just as in Monte–Carlo based methods; the stochastic Galerkin implementation (intrusive) requires heavy modifications of the code. However, most of these approaches fail in the case of "complex"

flows involving discontinuities with respect to the random variables (see [9,26]). There is active ongoing research on this topic.

Our main interest is the development of PC to conservation laws which are known to generate steep fronts and shocks. Let us illustrate this issue on an example.

1.1. Motivation 1

It is a classical hydrodynamical example (Euler system), Sod's test-case (see Fig. 1). Initially, for one deterministic realization, it consists of a Riemann problem (two different states separated by an interface) resulting in the appearance of a rarefaction wave, a contact discontinuity and a shock wave, see for example the middle curve of the top pictures of Fig. 1. We now consider an initially random interface position (a major issue in Inertial Confinement Fusion (ICF) for example) leading to a solution which will exhibit steep dependencies with respect to the uncertain initial interface position in the vicinities of both the contact discontinuity and the shock wave: Fig. 1 (top left) shows three possible realizations of the initial fluid density spatial distribution. Fig. 1 (top right) shows the corresponding three fluid density profiles at a later time $t > 0$. The stochastic Galerkin gPC method consists of a projection of the solution on the space spanned by a truncated orthogonal/orthonormal polynomial basis with respect to a probability measure: Fig. 1 (bottom right) shows this projection for a 5th order polynomial representation. The numerical approximation of the initial discontinuity in the random space gives birth to a severe Gibbs phenomenon leading to a negative approximation of the mass density: this is non-physical and can not be dealt with by any classical numerical schemes (see Remark 5.2.1). Consequently, for this example, the stochastic Galerkin gPC method fails at the first time step (depending on the numerical scheme). We give a more subtle example in Section 3.3.2 solving an inviscid Burgers'equation with uncertain *continuous* initial conditions: this example shows that dealing with non-linear equations inevitably leads to the same kind of problem for some $t > 0$.

1.2. Motivation 2

Even a non-intrusive method can become quite tricky on such problems. Let's suppose one wants to apply a Monte–Carlo method on our uncertain interface problem described in 1, on Fig. 1. It consists in generating N_{MC} samples of a random
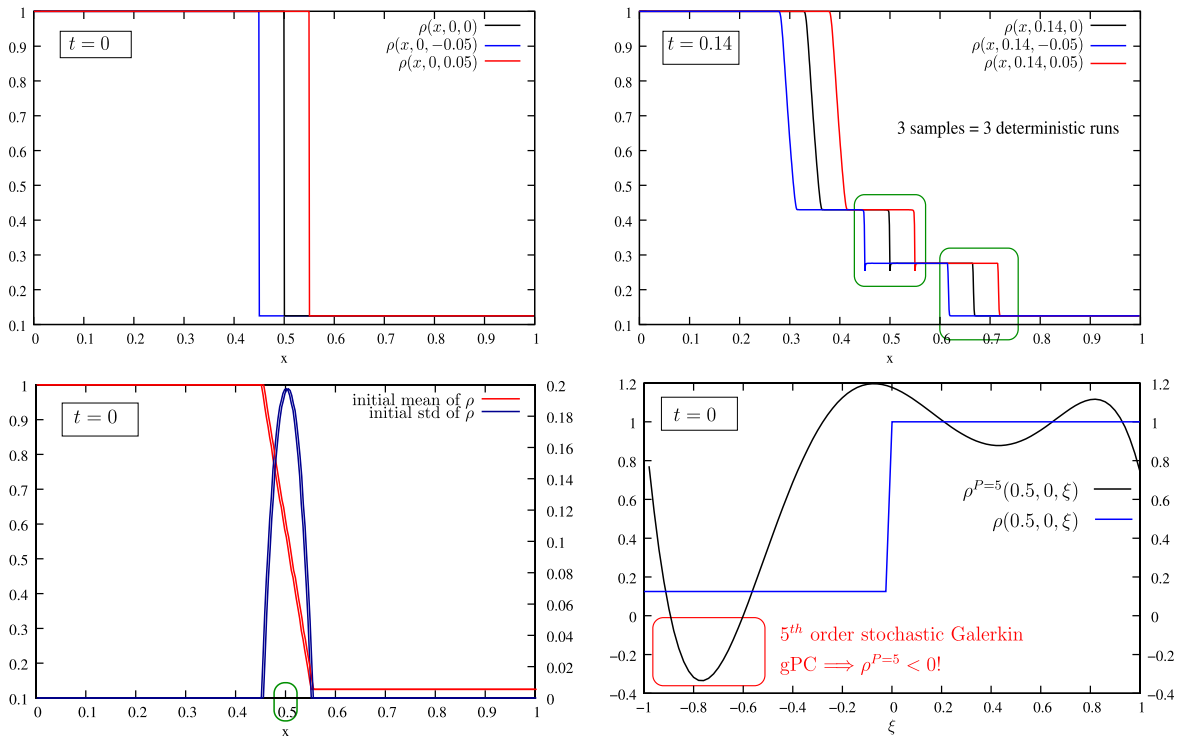
Fig. 1. One dimensional uncertain Sod test-case for compressible gas dynamics. Top pictures: Initial condition and solution at $t = 0.14$ for three realizations of the random interface position. These pictures give an idea of the numerical difficulties encountered due to the appearance of discontinuities. Bottom pictures: we apply the basic stochastic Galerkin gPC method: it consists in developing the solution on a truncated polynomial basis. The bottom left picture shows the initial mean and standard deviation of the density. It turns out that the discontinuity in the x-space reflects in the random space: the bottom right picture shows the density at $x = 0.5, t = 0$, with respect to the uncertain parameter ξ. The projection of the discontinuous density on the truncated smooth gPC basis of order 5, oscillates and gives birth to negative mass density.

variable, N_{MC} abscissas = N_{MC} positions of our interface for the N_{MC} runs of our "black box" code. The "black box" code implies a discretization of the physical domain in Nx cells. Without modifications of the code, the N_{MC} samples will be distributed between the cells of the grid concerned by the uncertainty. The direct consequence is a lack of accuracy in the sampling unless different grids are used for the different samples. It is also possible to use one unique grid for all the samples but increasing the accuracy of the MC method (by sampling more points) will imply refining the grid (at least in the vicinity of the uncertain interface). In both cases, for this kind of problem, even with a non-intrusive method, the UQ method and the "black box" code can not be independent. This is why we will focus on stochastic Galerkin methods. Several directions, for stochastic Galerkin methods, have been investigated in order to reduce the Gibbs phenomenon due to polynomial order truncation, among others: Haar wavelets [26], Multi-Resolution Analysis [18], ME-gPC [41,20,19,21,22] or ENO-like reconstructions in the random space [1]. All these methods rely on a special discretization of the random space. In the case of a moving discontinuity, adaptativity needs accurate interface tracking techniques, which are simple for 1-D problems, but become intricate in higher dimensions. In this case, the number of random subdomains can quickly become large. We want to avoid this kind of domain decomposition in the random space. This paper presents a new stochastic Galerkin method for systems of conservation laws enabling to bound the unphysical oscillations in the random space to a certain range imposed by the physics of the problem in the vicinity of discontinuities without adaptive method. We introduce a new variable, the *entropic variable* linked to the main variable through the entropy of the system and we carry on an analogy between extended thermodynamics of moments and Polynomial Chaos theory.

The starting point of our work is based on the observation that the mathematical structure of some well-known kinetic fluid models (see [7,30]) are really appropriate to introduce PC in conservation laws. We shall present this mathematical structure for general conservation laws. Once this done, it is easier to develop and justify the new PC algorithms. In this paper, we apply this methodology to two examples of interest, the inviscid Burgers' equation and the Euler system of compressible inviscid gas dynamics. Several authors already considered stochastic Burgers' equation, but in different frames: Mathelin and Lemaître considered the stationnary viscid Burgers' equation in [28] using *a posteriori* error analysis to h/p refine; Bell et al. [5] worked on algorithm refinement for the stochastic viscid Burgers' equation; Chen et al. [8] tackled the steady-state inviscid Burgers equation with source term with uncertainty carried on the initial conditions; Abgrall [1] tackled the same problem using ENO-like reconstruction in the random space before applying this method to the Euler system; Hou et al. [14] introduced a stochastic forcing term in the viscid Burgers' equation driven by Brownian Motion before tackling the stochastic incompressible Navier–Stokes equations driven by Brownian Motion. Authors mainly tackled fluid dynamics using adaptive methods: ME-gPC has been used to tackle the problem of long-term behavior for noisy incompressible flow past a cylinder, [40]. It has also been used to tackle supersonic compressible flows past a wedge with random inflow fluctuations or random oscillations around its apex [21]. More recently, Multi-Element Probabilistic Collocation Method has been applied to supersonic compressible flows past a wedge with rough surface [22]. In our work, the algorithms are based on well-posed hyperbolic systems of conservation laws, the schemes are conservative and the Gibbs phenomena can be interpreted and controlled by means of the mathematical entropy of the system.

The paper is organised as follows. In Section 2.1, a brief outline of the presentation is provided. A parallel between Kinetic theory/theory of moments [7,30] and Polynomial Chaos (PC) representations is established in Section 2. Thus a new UQ method for systems of conservation laws is introduced with its properties. In Section 3, the method is applied to a simplified scalar problem: the inviscid Burgers' equation. We construct an original scheme for the calculation of the discrete solutions and we present results in 1-D and 2-D random dimensions, comparing our new approach to the stochastic Galerkin gPC method. The new approach bounds the oscillations due to Gibbs phenomenon and is more accurate than the stochastic Galerkin gPC method. Finally, we generalize the approach to compressible fluid dynamic in Eulerian coordinates. Numerical results are presented in a last section, in particular, the uncertain Sod test case of Fig. 1, for which the stochastic Galerkin gPC method fails, is solved with the new method.

2. Modeling uncertainties in conservation laws

Let us consider a general system of conservation laws

$$\partial_t u + \partial_x f(u) = 0, \tag{1}$$

where $u = u(\mathbf{x}, t) \in \mathbb{R}^n$ is the solution, $\mathbf{x} \in \mathcal{D} \subset \mathbb{R}^d$ is the space coordinate, t is the time coordinate and the flux is $f : \mathbb{R}^n \to \mathbb{R}^n$. We suppose furthermore that there exists a pair of real-valued mappings (s, g) for continuous solution of system (1) such that

$$\begin{array}{cc} \mathbb{R}^n \to \mathbb{R}, & \mathbb{R}^n \to \mathbb{R}, \\ u \to s(u) & u \to g(u) \end{array} \quad \text{and} \quad \partial_t s(u) + \partial_x g(u) = 0. \tag{2}$$

The pair (s, g) is called an *entropy–entropy flux pair*. If, in addition, $u \to s(u)$ is strictly convex, then, the existence of (s, g) implies the hyperbolicity of system (1), see [34] or [12] for more mathematical details.

We wish to introduce some measure of uncertainty due to initial conditions, model constants or boundary conditions, etc. So we consider that our system no longer depends only on $\mathbf{x}$ and t coordinates but also on a new variable $\omega \in \Omega$. Ω is the set in which ω takes its values. The unknown function $u(\mathbf{x}, t, \omega)$ is a solution of the following system

$$\partial_t u(\boldsymbol{x}, t, \omega) + \partial_x f(u(\boldsymbol{x}, t, \omega)) = 0. \tag{3}$$

At this stage, this system can be interpreted as an infinite number of decoupled systems like (1) for the realizations $\omega_1, \omega_2, \ldots$

In the UQ approach, probabilities are introduced to model the fact that all events ω are not equivalent. This is done by defining a probability measure $d\mathcal{P}(\omega)$ such that $\int_\Omega d\mathcal{P}(\omega) = 1$. Then the quantity of interest is the product of the unknown function u with the weight of the "event" ω,

$$u(\boldsymbol{x}, t, \omega) d\mathcal{P}(\omega). \tag{4}$$

It is important to notice that the structure of the problem is very close to kinetic models. In the Kinetic theory (see [7,30]), one describes the state of a gas by the phase density function $f(\boldsymbol{x}, t, \boldsymbol{v})$ such that $f(\boldsymbol{x}, t, \boldsymbol{v}) d\boldsymbol{v}$ is the number of atoms at the location $\boldsymbol{x}$ at the time t with velocity $\boldsymbol{v} + d\boldsymbol{v}$. It is usual in [7,30] to define fluid models by taking moments of the kinetic model[1] giving birth to well-known systems depending on the number of moments (Euler, Navier–Stokes, Grad's 13 Moments Theory, …, see [30] (p. 5 or pp. 19–21 for examples)). In order to adapt this theory to our problem, we need to take the moments of (4) to construct a new system of conservation laws: the PC theory, by introducing a polynomial basis orthonormal with respect to the *probability density function* (pdf) associated to $d\mathcal{P}(\omega)$, enables addressing this issue.

2.1. The Polynomial Chaos theory

The Polynomial Chaos (PC) method is a non-statistical method used to solve stochastic differential (SDE) and stochastic partial differential equations (SPDE). PC and its generalized version (gPC) methods have recently emerged as a reliable and efficient numerical tool for numerous engineering applications with Gaussian or non-Gaussian parametric uncertainty, among others [32,45,24,29,39,25,16]. It is based on introducing *geometry* and *coordinates* in the probability space on which input and solution uncertainty are modeled. The efficiency of this approach depends crucially on the judicious choice of "coordinates" in probability space. [35] pioneered the computational use of the PC expansion method. PC expansions are based on the homogeneous chaos theory of [42]. They allow high-order deterministic approximation of random fields and appear to exhibit spectral convergence in many cases. gPC expansions, also called Wiener–Askey chaos expansions, that are orthogonal with respect to non-Gaussian probability measures were first employed in computational algorithms by [43], following developments in probability by [31,33], and on orthogonal polynomials by [3,17]. In gPC, the polynomials are chosen from the hypergeometric polynomials of the *Askey family* where the underlying random variables are not restricted to Gaussian random variables.

In the following, the mathematical fundations of PC theory will be briefly exposed and the reader should refer to [11] for more details on the subject. We give a general framework for the expository purposes, it is not indispensable for the understanding of the algorithms of the practical sections. Stochastic mathematical models are based on a *probability space* $(\Omega, \mathcal{A}, \mathcal{P})$ where Ω is the event space, $\mathcal{A} \subset 2^\Omega$ its σ-algebra, and $\mathcal{P}$ its probability measure. We consider a random field $u(\omega)$, i.e. mappings $u : \Omega \to V$ from the probability space into a function space V. If $V = \;$, $u(\omega)$ are random variables, and if V is a function space over a time and/or space interval, random fields are stochastic processes. V is a Hilbert space with dual V', norm $\|\cdot\|$ and inner product $(\cdot, \cdot) : V \times V \to\;$. As V is densely embedded in V', we abuse notation and denote by $(\cdot, \cdot)$ also the $V \times V'$ duality pairing. In practice, in the following sections, we will take $V = V' = L^2(\Omega, \mathcal{A}, \mathcal{P})$: we will consider second-order random fields, i.e. $u : \Omega \to V$ is a *second-order* random field over V, if

$$\|u\|^2 = \;(u, u) = \|u\|^2_{L^2(\Omega, \mathcal{A}, \mathcal{P})} < \infty,$$

where $\;$ denotes the expectation of a random variable $Y \in L^2(\Omega, \mathcal{A}, \mathcal{P})$, and is defined by

$$Y = \int_{\omega \in \Omega} Y(\omega) d\mathcal{P}(\omega).$$

The gPC approach is a means of representing second-order random fields $u(\omega)$ parametrically through a set of i.i.d. (independent identically distributed) random variables $\{\xi_j(\omega)\}_{j=1}^N, N \in\;$, through the events $\omega \in \Omega$:

$$u(\omega) = \sum_{k=0}^\infty u_k \phi_k(\boldsymbol{\xi}(\omega)). \tag{5}$$

This is an infinite series in which $\{\phi_j(\boldsymbol{\xi}(\omega))\}$ are mutually orthonormal polynomials in terms of a zero-mean random vector $\boldsymbol{\xi} := \{\xi_j(\omega)\}_{j=1}^N$, satisfying the orthonormality relation

$$\langle \phi_i \phi_j \rangle = \delta_{ij}, \tag{6}$$

where $\langle \cdot, \cdot \rangle$ denotes the ensemble average. We note that the modal coefficients u_k are purely deterministic quantities, they are independent of ω. The number of random variables $N \in\;$ is in general infinite, so is the index in (5). In practice, however, we need to retain a finite set of random variables, i.e. to $\{\xi_j\}_{j=1}^N$ with $N < \infty$, and a finite-term truncation of (5).

---

[1] For example, the mass density is $\rho = \int f d\boldsymbol{v}$ and the momentum density is $\rho\boldsymbol{u} = \int f \boldsymbol{v} d\boldsymbol{v}$.

The inner product in (6) is based on the measure $w(\xi)$ of the random variables:

$$\langle f(\xi)g(\xi)\rangle = \int_{\omega\in\Omega} f(\xi(\omega))g(\xi(\omega))d\mathcal{P}(\omega) = \int f(\xi)g(\xi)w(\xi)d\xi = \int f(\xi)g(\xi)\mathrm{d}_w\xi = \int fg\mathrm{d}w, \tag{7}$$

with $w(\xi)$ denoting the density of $\mathrm{d}\mathcal{P}(\omega)$ with respect to the Lebesgue measure $\mathrm{d}\xi = \mathrm{d}\xi_1\ldots\mathrm{d}\xi_N$[2] and with integration taken over a suitable domain, determined by the range of ξ.

In Eq. (5), there is a one-to-one correspondence between the type of the polynomial $\{\phi\}$ and $w(\xi)$. Indeed, the weighting function of $\{\phi\}$ has a similar form as $w(\xi)$. For instance, the weighting function of Hermite orthogonal polynomials corresponds to $\exp\left(-\frac{1}{2}\xi^T\xi\right)/(2\pi)^{N/2}$, and is the same as the probability density function (pdf) of the N-dimensional Gaussian random variables ξ. Hence, the classical Wiener Polynomial Chaos is an expansion of Hermite polynomials in terms of Gaussian random variables. A correspondence between orthogonal polynomials and random variables was first established by [31,33]. It is worth mentioning that the optimal choice of the gPC basis remains an open question. Indeed the type of distribution of the SPDE solution is not known most of the time. When the random input distribution is known, one can choose the corresponding polynomial from the Askey family as the gPC basis. We emphasize that this choice is not indisputable. The optimality is only guaranteed for the stochastic inputs. For non-linear problems, it is not clear that an optimal representation of the inputs is necessarily optimal for the entire problem.

The expansion in (5) is truncated to a finite-dimensional space based on a "finite-dimensional noise assumption" that is accomplished by characterizing the probability space by a finite number N of random variables. Further, the highest order M of the polynomials $\{\phi\}$ is selected based on accuracy requirements. Consequently, the finite-term expansion takes the form

$$u(\omega) = \sum_{j=0}^{P} u_j\phi_j(\xi(\omega)), \tag{8}$$

where $\xi = (\xi_1,\cdots,\xi_N)^T$ is an N-dimensional random vector with ξ_i independent of ξ_j for all $1 \leqslant i\neq j \leqslant N$. The multi-dimensional gPC expansion is constructed as the tensor product of the corresponding one-dimensional expansion. With this structure, the total number of expansion terms P is,

$$P = (N + M)!/(N!M!) - 1. \tag{9}$$

In order to compute the coefficients, the classical approach consists in substituting the gPC expansion (5) into the SPDE to represent both the solution and the random inputs. The new system is then projected (with a Galerkin-type projection) onto the truncated orthonormal polynomial basis. This projection leads to a *deterministic* coupled system of P differential equations. After solving for the deterministic coefficients u_k, we have an explicit functional representation (in random space) of the solution process. It is then possible to perform a number of analytical operations on the stochastic solution. Moments, sensitivity analysis, confidence intervals and pdf of the solution can be evaluated. Due to the orthonormality of the modes, the moments can be easily computed. For instance, the *mean* solution is contained in the expansion term with zero-index. The *second moment*, i.e. the *covariance function* is given by a linear combination of the modal fluctuations. We have:

$$\mu_u = \langle u(\omega)\rangle = u_0$$

$$\sigma_u^2 = \langle(u(\omega) - u_0)^2\rangle = \sum_{j=1}^{P}[u_j^2\langle\phi_j^2\rangle] = \sum_{j=1}^{P} u_j^2.$$

2.2. Intrusive Polynomial Moment Method (IPMM) for systems of conservation laws

We now apply the above material to our problem. In the stochastic Galerkin gPC method (sG-gPC), the polynomial moments of u are defined as $u_k = \int u\phi_k\mathrm{d}w$ for $k \in \{0,\ldots,P\}$ and the question of the closure is answered by taking $u \approx \Pi_P u = \sum_{k=0}^{P} u_k\phi_k$ where $(\phi_k)_{k\in\{0,\ldots,P\}}$ is a polynomial basis of $L^2(\Omega)$, orthonormal with respect to the pdf w. The convergence of the sum with respect to P is guaranteed by Cameron–Martin theorem [6].

In [30] (pp. 29–32), a new variable v is introduced, the *entropic variable*, defined by $v = \nabla_u s(u) \in \mathbb{R}^n$, where s is the entropy defined by (2). The transformation $v \to u(v)$ is one-to-one. The key idea of our approach consists of defining a second family of coefficients $v_k = \int v\phi_k\mathrm{d}w, \forall k \in \{0,\ldots,P\}$, polynomial moments of v, so that

$$v \approx \Pi_P v = \sum_{k=0}^{P} v_k\phi_k. \tag{10}$$

Using the bijection between u and v, the moments of u are related to the moments of v as follows:

$$\forall k \in \{0,\ldots,P\}, u_k = \int u(\Pi_P v)\phi_k\mathrm{d}w = \int u\left(\sum_{j=0}^{P} v_j\phi_j\right)\phi_k\mathrm{d}w. \tag{11}$$

---

[2] *Notations:* $\mathrm{d}_w\xi = w(\xi_1,\ldots,\xi_N)\mathrm{d}\xi_1\ldots\mathrm{d}\xi_N$.

The new system of polynomial moments that we consider is:

$$\partial_t \begin{pmatrix} \int u\left(\sum_{i=0}^{P} v_i \phi_i\right)\phi_0 dw \\ \cdots \\ \int u\left(\sum_{i=0}^{P} v_i \phi_i\right)\phi_P dw \end{pmatrix} + \partial_x \begin{pmatrix} \int f\left(u\left(\sum_{i=0}^{P} v_i \phi_i\right)\right)\phi_0 dw \\ \cdots \\ \int f\left(u\left(\sum_{i=0}^{P} v_i \phi_i\right)\right)\phi_P dw \end{pmatrix} = 0 \tag{12}$$

which we rewrite in a more compact notation

$$\partial_t U^P + \partial_x F(U^P) = 0 \quad \text{with } U^P = (u_0, \ldots, u_P)^t \in \,^{(P+1)\times n}. \tag{13}$$

We should rigorously write $U^P = U(V^P)$ where $V^P = (v_0, \ldots, v_P)^T$ but we keep this implicit to simplify the notations. We rely on the theoretical framework of Section 2.1 (and more particularly on Cameron–Martin theorem [6]) to suppose that for P large enough, Eqs. (12) and (13) are a good representation of Eq. (4).

Remark 2.2.1. The classical approach is recovered by taking $s(u) = \frac{u^2}{2}$ (scalar case). In this case, we obtain $v = \nabla_u s(u) = u$ and developing v or u onto the polynomial basis is equivalent.

Following the notations of [30] (pp. 33–39), we refer to Eqs. (12) and (13) as the P-truncated subsystem of Eq. (4). Different properties of the method will be presented in the following. In particular, we explain how V^P can be computed given U^P.

2.3. Properties of the P-truncated subsystem

These following properties can be directly derived from the properties stated in [30].

Property 2.3.1 (Hyperbolicity). *Assuming the system (4) is hyperbolic, then the P-truncated subsystem (12) is also hyperbolic $\forall P \in$. There exists an entropy–entropy flux pair (S,G) for the P-truncated subsystem (12) which can be derived from the entropy–entropy flux pair (s,g) of (4). We have:*

$$S = \int s\, dw, \quad G = \int g\, dw.$$

The proves are given in [30] (pp. 33–34 and pp. 201–205).

Remark 2.3.1 (*Entropy inequality*). The entropy–entropy flux pair is such that for smooth solutions $\partial_t S(U(x,t)) + \partial_x G(U(x,t)) = 0$. However, discontinuous solutions must satisfy $\partial_t S(U(x,t)) + \partial_x G(U(x,t)) < 0$. By integrating over the whole space $\mathcal{D}$ and in between instants $t = 0$ and $t = T$, we obtain $\int_{\mathcal{D}} S(U(x,T)) dx \leqslant \int_{\mathcal{D}} S(U(x,0)) dx$, and finally,

$$\int_{\omega \in \Omega} \int_{\mathcal{D}} s\left(u\left(\sum_{k=0}^{P} v_k(x,T)\phi_k(\xi(\omega))\right)\right) dx d\mathcal{P}(\omega) \leqslant \int_{\omega \in \Omega} \int_{\mathcal{D}} s\left(u\left(\sum_{k=0}^{P} v_k(x,0)\phi_k(\xi(\omega))\right)\right) dx d\mathcal{P}(\omega), \tag{14}$$

which is an *a priori* inequality the solution will have to satisfy.[3]

In the following, this inequality will be used with particular entropies s and we will explain how numerical solutions satisfying it can be controlled.

Remark 2.3.2 (*Non-linear projection*). The new approach can be understood as a non-linear projection: if the exact solution is $u = \sum_{k=0}^{\infty} u_k \phi_k$, the solution $\Pi_P u = \sum_{k=0}^{P} u_k \phi_k$ from sG-gPC is such that

$$\begin{cases} \text{for } 0 \leqslant k \leqslant P \\ \int (\Pi_P u)\phi_k dw = \int u \phi_k dw = u_k \end{cases} \text{with} \begin{cases} \text{for } P < k \\ \int (\Pi_P u)\phi_k dw = 0. \end{cases}$$

On the other hand, the solution $u\left(\sum_{k=0}^{P} v_k \phi_k\right)$ from IPMM is such that

$$\begin{cases} \text{for } 0 \leqslant k \leqslant P \\ \int u\left(\sum_{j=0}^{P} v_j \phi_j\right)\phi_k dw = \int u \phi_k dw = u_k \end{cases} \text{with a priori} \begin{cases} \text{for } P < k \\ \int u\left(\sum_{j=0}^{P} v_j \phi_j\right)\phi_k dw \neq 0. \end{cases}$$

By construction, the method selects one solution, $u\left(\sum_{k=0}^{P} v_k \phi_k\right)$, such that

---

[3] Note that in this paper, the entropy denotes the mathematical entropy which is strictly convex and tends to decrease for a closed system. For example, for the Euler system, the mathematical entropy is the opposite of the physical entropy.

$$\begin{cases} \text{for } 0 \leqslant k \leqslant P \\ \int u\left(\sum_{j=0}^{P} v_j\phi_j\right)\phi_k \mathrm{d}w = u_k \end{cases} \quad \text{and} \quad \int \int_{\mathcal{D}} s\left(u\left(\sum_{k=0}^{P} v_k(x,T)\phi_k(\xi)\right)\right)\mathrm{d}x\mathrm{d}_w\xi \leqslant \int \int_{\mathcal{D}} s(x,0,\xi)\mathrm{d}x\mathrm{d}_w\xi.$$

This ensures a certain control of the oscillations, depending on the expression of the entropy. For example, suppose the entropy defines a particular definition domain for the solution,[4] say $s(u) = -\ln(u - u_*)$ in the case of a scalar equation. The solution of IPMM $u(\Pi_P v)$ is regular: suppose that at some fixed time $T > 0$, the solution is such that for $(x^*, \xi^*), u(\Pi_P v(x^*, T, \xi^*)) \leqslant u_*$ (one possible consequence of an oscillatory-like behavior). Then it violates (14) since $s(u(\Pi_P v(x^*, T, \xi^*)))$ diverges. IPMM finds $u\left(\sum_{k=0}^{P} v_k\phi_k\right)$ such that the P first moments approximate those of the analytical solution and such that (14) is satisfied, implying that the solution is constrained to certain bounds defined through the expression of the entropy.

The last important point of this section concerns the computation of V^P from U^P: [30] (pp. 218–220) provides a procedure to compute V^P from U^P ensuring the equivalence between the resolution of (12) and the resolution of (4).

Property 2.3.2. (**Minimization of entropy**) *For a given U^P, let us define a convenient Legendre transform of the entropy*

$$T(W^P) = -\langle U^P, W^P \rangle + \langle U(W^P), W^P \rangle - S(U(W^P)). \tag{15}$$

Then V^P, such that $U^P = U(V^P)$, is the unique minimum of T.

Indeed, we have

$$\nabla_{W^P} T(W^P) = -U^P + U(W^P) + \nabla_{W^P} U(W^P) W^P - \nabla_{W^P} U(W^P) \underbrace{\nabla_U S(U(W^P))}_{W^P} = -U^P + U(W^P). \tag{16}$$

Consequently, $\nabla_{W^P} T(W^P) = 0$ if $U^P = U(W^P)$ and this equality is satisfied by V^P. Besides,

$$\nabla_{W^P} T(W^P) = -U^P + U(W^P),$$
$$\nabla^2_{W^P, W^P} T(W^P) = \nabla_{W^P} U(W^P) = \nabla^2_{W^P, W^P} S^*(W^P) > 0 \tag{17}$$

where $S^* = \int s^* \mathrm{d}w$ is stricly convex: s^* is by definition the entropy of the system satisfied by the entropic variable v (see [30] (pp. 33–35)). Consequently, T is strictly convex and assuming there exists a minimum for T, then the minimum is unique.

In practice, the minimization of the functional is done using a Newton algorithm. All the conditions are satisfied so that we have a quadratic convergence of the algorithm: the initial guess is V_i^n (from the previous time step), the functional is strictly convex and we have analytical expressions of its derivatives. The different steps of the algorithm are as follow:

$$\begin{cases} -\text{with } W^0 = V_i^n \text{ as an initial guess(this is common procedure for solving time dependent problems),} \\ -W^{k+1} = W^k - [\nabla^2_{WW} T(W^k)]^{-1} \nabla_W T(W^k), \\ -\|W^{k+1} - W^k\| < \epsilon_{Newt} = (10^{-10} : \text{numerical results of this paper are obtain with such an accuracy}), \\ -W^k \leftarrow W^{k+1}. \end{cases}$$

Remark 2.3.3. The Legendre transform of the entropy T is strictly convex. In practice, we have observed that this is not enough. In fact, we have noticed that T must be α-convex to be able to calculate V^P from U^P.

Let's take a simple example to illustrate Remark 2.3.3. We consider the trivial equation $u(v) = a$ with $s(u) = -\ln(u)$ so that the solution is $v = -\frac{1}{a}$. We want to solve this problem by minimizing the functional $T(v) = 1 + \ln(-v) + av$. It is a classroom exercise to discuss the two following cases:

- If $a > 0, T$ is not α-convex and T has no minimum (see Fig. 2).
- If $a < 0, T$ is α-convex and T has a unique minimum which gives the solution (see Fig. 2).

This has important consequences from a numerical point of view as the minimization algorithm could fail to find a minimum. In practice, the functionnal is α-convex if P is large enough. In this case, the Newton algorithm used to compute the minimum converges.

3. Burgers' equation: 1D random dimension

One of the simplest conservation laws is the inviscid Burgers' equation in 1D for the physical variable ($n = 1$) and 1D for the uncertain variable ($N = 1$)

---

[4] It is the case for compressible gas dynamics in Lagrangian coordinates for example, as $s(\tau, \epsilon) = -\ln(\tau^{\gamma-1}\epsilon)$ and the product in the logarithm (specific volume$^{\gamma-1} \times$ internal energy) can not tend to zero or take negative values. Same idea for Burgers equation of Section 3 with the entropy $s(u) = -\ln(u - u_-)$ and its variants.
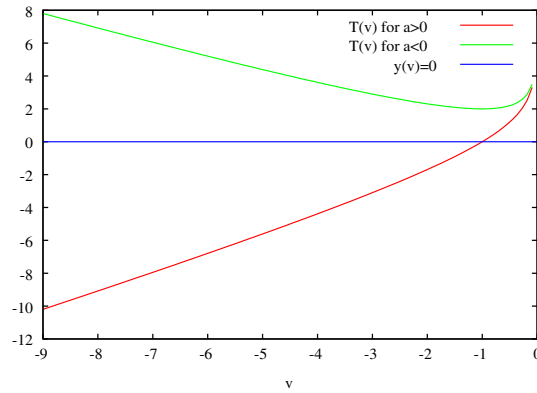
Fig. 2. Example of function α-convex: if $a < 0$, T has a finite minimum whereas if $a > 0$, T is only strictly convex and its minimum goes to $-\infty$.

$$\partial_t u(x, t, \xi) + \partial_x \frac{u^2(x, t, \xi)}{2} = 0. \tag{18}$$

This equation constitutes a first step toward compressible gas dynamics and has been studied extensively, see for example [4] in the context of turbulent flows. One important property of (18) is that except for very special cases,[5] shocks will develop in the solution even for smooth initial conditions. In the following, we denote by t^* the time of formation of the last shock. Shocks propagating in the x-space will generate discontinuities in the random space leading to P-convergence problem.

For this equation, one can calculate analytical solutions from the initial conditions. For the expression of the initial conditions and their respective analytical solutions, we refer the reader to Appendix A. This system has an infinite number of entropy–entropy flux pairs (see [12]). In this paper, three different ones are compared:

$$
\begin{aligned}
s_0(u) &= \frac{u^2}{2} & |v = \nabla_u s_0(u) = u, \\
s_1(u) &= -\ln(u - u_-) & |v = \nabla_u s_1(u) = -\frac{1}{u - u_-}, \\
s_2(u) &= -\ln(u - u_-) - \ln(u_+ - u) & |v = \nabla_u s_2(u) = -\frac{1}{u - u_-} + \frac{1}{u_+ - u}.
\end{aligned}
\tag{19}
$$

For the first entropy s_0, $u = v$ and the system is (22). The two other entropies depend on parameters, u_- and u_+ which will be chosen afterward. There exists a one-to-one transformation to obtain u from v:

$$
\begin{aligned}
u(v) &= v & \text{with entropy } s_0, \\
u(v) &= \frac{-1 + v u_-}{v} & \text{with entropy } s_1, \\
u(v) &= -\frac{1}{v} + \frac{u_- + u_+}{2} + \frac{\sqrt{(u_- - u_+)^2 v^2 + 4}}{2v} & \text{with entropy } s_2.
\end{aligned}
\tag{20}
$$

Remark 3.0.4. The entropies s_1 and s_2 have singularities at $u = u_-$ and $u = u_+$. At a continuous level, inequality (14) gives some control of the solution u near the singularities. The discrete counterpart of inequality (14) will force the solution within the domain defined by the two bounds.

Remark 3.0.5. Burgers' equation being a scalar conservation law, there exists a maximum principle for the entropic solution (see [34] (II p. 2)). Consequently, for scalar conservation laws, and here Burgers' equation, once the initial condition is given, it is possible to choose the parameters u_- and u_+ according to the domain invariants.

We consider two initial conditions, see Appendix A. The first one is piecewise linear (IC_1) and the second one is its smoother counterpart (IC_2). See Fig. 3 for the profiles of the initial conditions IC_1 (left) and IC_2 (right) for one realization of the parameter ξ.

In both cases, after t^*, the solutions are discontinuous with a step-function-like behavior and the discontinuity velocity is $D = \frac{u_R + u_L}{2}$ where u_R and u_L are the right and left states of u (the velocity is obtained thanks to the Rankine–Hugoniot relations). Besides, the theoretical value of $t^*(\xi)$ is known

---

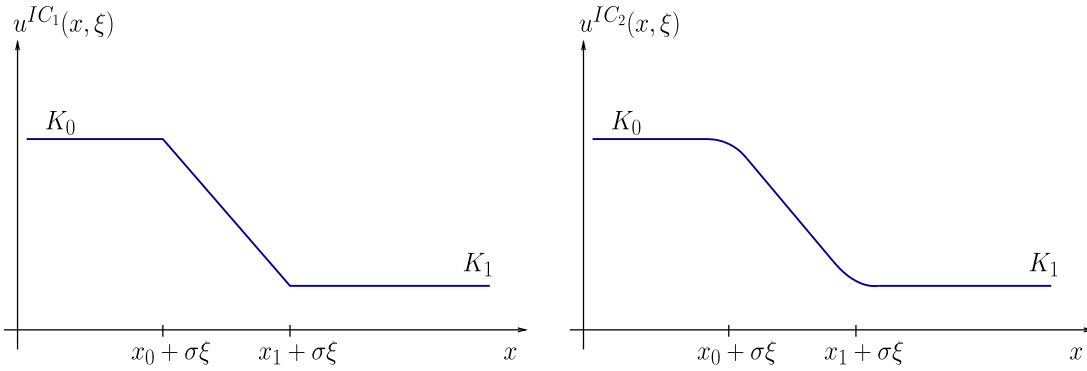[5] Which will not be part of this study.

Fig. 3. Initializations for test-cases IC_1 (left) and IC_2 (right).

$$t^*(\xi) = -\frac{1}{\inf\limits_{x\in\mathcal{D}}\left(\frac{\mathrm{d}u}{\mathrm{d}x}(x,0,\xi)\right)}.$$ (21)

For both initializations IC_1 and IC_2, $u(x,0,\xi)$ is a translation of $u(x,0,0)$ so that the discontinuity velocity D and t^* do not depend on the random variable ξ. According to (21),

$$\text{for } IC_1 : t^* = -\frac{x_1 - x_0}{K_1 - K_0}, \text{ and for } IC_2 : t^* = -\frac{1}{-\frac{b^2}{3a}+c}.$$

The particularity of the IC_2 case is that the first derivatives of the solution are smooth for $t < t^*$ so that the P-convergence is reached at $t = 0$ for low polynomial developments. However, the dynamics will become more challenging as t tends to t^*.

3.1. Choice of the probability laws

The different remarks and properties of the latter sections are independent of the choice of the probability law and of the orthonormal polynomial basis: the structure of the algorithms enables us to take into account a general framework. In the following examples, for the sake of simplicity, we choose ξ to parametrize a *uniform* random variable of zero mean on $[-0.2, 0.2]$ for both 1D random initializations: we actually use $\sigma\xi$ in the following with $\sigma = 0.2$ and $\xi \in [-1,1]$. The same choice is made for the 2D random initializations as (ξ_0, ξ_1) will be i.i.d. uniform laws on $[-1,1]$ and we will take $\sigma_0 = 0.1$ and $\sigma_1 = 0.2$. The polynomial basis is the orthonormal Legendre basis for the 1D case and a tensorised Legendre basis for the 2D one, see [36].

We now compare the stochastic Galerkin gPC method with the Intrusive Polynomial Moment Method.

3.2. The stochastic galerkin gPC method (sG-gPC)

In the classical approch, the main variable u is developed on the polynomial basis. We consider that $u(x,t,\xi) \approx \Pi_P u(x,t,\xi) = \sum_{k=0}^{P} u_k(x,t)\phi_k(\xi)$ with

$$u_k(x,t) = \int u(x,t,\xi)\phi_k(\xi)\mathrm{d}_w\xi \quad \forall k \in \{0,\ldots,P\}.$$

We introduce the development of u in (18) and perform a Galerkin Projection on the polynomial basis. We obtain:

$$\partial_t \begin{pmatrix} u_0 \\ \ldots \\ u_P \end{pmatrix} + \frac{1}{2}\partial_x \begin{pmatrix} \sum_{i,j=0}^{P} u_i u_j c_{i,j,0} \\ \ldots \\ \sum_{i,j=0}^{P} u_i u_j c_{i,j,P} \end{pmatrix} = 0$$ (22)

where $c_{i,j,k} = \int \phi_i(\xi)\phi_j(\xi)\phi_k(\xi)\mathrm{d}_w\xi$ and we suppose that the polynomial basis is orthonormal. In our formalism, this approach is equivalent to take $s(u) = \frac{u^2}{2}$ so that $v = u$. A consequence of Property 2.3.1 is that the system (22) is hyperbolic (the proof can also be demonstrated using the same kind of arguments of [8]). In the following subsection, we present the numerical scheme used to solve the discrete version of (22).

3.2.1. Roe Scheme for sG-gPC

A finite volume method is employed, which is well adapted as (22) is a non-linear system of conservation laws. It is possible to use a Roe solver for the resolution. One possible Roe matrix for the problem is $A(U,V) = \nabla_u f(\frac{U+V}{2})$ whose general term is $A(U,V)_{i,j} = \frac{1}{2}\sum_{k=0}^{P}(u_k + v_k)c_{k,i,j}$. Indeed, the three Roe conditions (see [12]) for the matrix are satisfied:

- $A(U,V)$ has all its eigenvalues in ⸱⸱⸱ and a complete basis of eigenvectors as the system is hyperbolic.
- Besides, by construction $\forall U \in \mathbb{R}^{P+1}, A(U,U) = \nabla_u f(U)$.
- And finally, $\forall (U,V) \in \mathbb{R}^{P+1} \times \mathbb{R}^{P+1}, f(U) - f(V) = A(U,V)(U - V)$ because of the quadratic form of the flux.

The numerical flux is then

$$f_{j+1/2}^n = \frac{1}{2}(f(U_j^n) + f(U_{j+1}^n)) - \frac{1}{2}|A(U_j^n, U_{j+1}^n)|(-U_j^n + U_{j+1}^n)$$

where by definition, $|A| = P_1|\Lambda|P_2$ with $|\Lambda| = diag(|\lambda_1|, \ldots, |\lambda_n|)$; P_1 and P_2 are the base-changing matrices such that $A = P_1 \Lambda P_2$ with $\Lambda = diag(\lambda_1, \ldots, \lambda_n)$. A Roe scheme is stable under CFL condition, $\max_{k \in \{0 \ldots P\}} |\lambda_k| \frac{\Delta t}{\Delta x} \leqslant CFL$ and is conservative. An entropic correction is possible: the one we use is such that we take $\max(|\lambda_k|, \epsilon)$ (with $\epsilon > 0$) instead of $|\lambda_k|$ in the diagonalisation of $|A|$.

3.3. The Intrusive Polynomial Moment Method (IPMM)

We consider now a general entropy s. Every convex function s defines an entropy–entropy flux for Burgers' equation. We develop the entropic variable $v = \nabla_u s(u)$ onto the polynomial basis, use the bijective transformation $v \to u(v)$ and a Galerkin projection on the orthonormal basis to obtain:

$$\partial_t \begin{pmatrix} \int u\left(\sum_{i=0}^P v_i(x,t)\phi_i(\xi)\right)\phi_0(\xi)d_w\xi \\ \cdots \\ \int u\left(\sum_{i=0}^P v_i(x,t)\phi_i(\xi)\right)\phi_P(\xi)d_w\xi \end{pmatrix} + \frac{1}{2}\partial_x \begin{pmatrix} \int u^2\left(\sum_{i=0}^P v_i(x,t)\phi_i(\xi)\right)\phi_0(\xi)d_w\xi \\ \cdots \\ \int u^2\left(\sum_{i=0}^P v_i(x,t)\phi_i(\xi)\right)\phi_P(\xi)d_w\xi \end{pmatrix} = 0 \tag{23}$$

The dependence of (23) with respect to the choice of s is in the definition of the bijection $v \to u(v)$. From Section 2.3, we know that the system (23) is hyperbolic.

3.3.1. Discretization for IPMM

The algorithm needs two steps to compute for each cell j and time step $n + 1$ the moments of $v, V_j^{n+1} = (v_{0,j}^{n+1}, \ldots, v_{P,j}^{n+1})^T$, from the moments of v at time step $n, V_j^n = (v_{0,j}^n, \ldots, v_{P,j}^n)^T$. From V_j^n, we have $U_j^n = (u_{0,j}^n, \ldots, u_{P,j}^n)^T$ using the relation $u_{k,j}^n \approx \int u\left(\sum_{i=0}^P v_{i,j}^n \phi_i\right)\phi_k dw$. We go from U_j^n to U_j^{n+1} by an iteration of our numerical scheme (first step) and from U_j^{n+1} to V_j^{n+1} by the minimization algorithm of Remark 2.3.2 (second step). In practice, the integrals are computed by numerical quadrature. In this paper, we do not study the influence of the number of quadrature points. In our examples, the number of quadrature points is large enough to consider the integrals are exactly computed (typically, for the heavier computations (13th order truncation), a level in Clenshaw–Curtis rule up to 7 is invoked).

First step: we wish to discretise the system (23) with a finite volume approach $U_j^{n+1} = U_j^n - \frac{\Delta t}{\Delta x}(F_{j+1/2}^n - F_{j-1/2}^n)$. The flux is not quadratic anymore and the previous simple Roe scheme can not be used. For all the Burgers' test-cases considered, an upwinded Roe scheme is enough (see Appendix B), so that the accuracy and the computational cost of the numerical schemes for sG-gPC and IPMM are comparable.

Second step: it concerns the computation of $V_j^{n+1} = (v_{0,j}^{n+1}, \ldots, v_{P,j}^{n+1})^t$ from $U_j^{n+1} = (u_{0,j}^{n+1}, \ldots, u_{P,j}^{n+1})^t$ at the end of a time step. The functional to minimize in each cell and at each time step is

$$T(W_j^{n+1}) = -\sum_{k=0}^P u_{k,j}^{n+1} w_{k,j}^{n+1} + \int u\left(\sum_{t=0}^P w_{t,j}^{n+1}\phi_t\right)\sum_{k=0}^P w_{k,j}^{n+1}\phi_k dw - \int s\left(u\left(\sum_{t=0}^P v_{t,j}^{n+1}\phi_t\right)\right)dw. \tag{24}$$

In the following numerical results, we use a Newton-type algorithm for the minimization procedure as described in Property 2.3.2. The integrals in (24) are approximated with numerical quadratures. Let N_q be the number of quadrature points; then, if $N_q \leqslant P$, the minimization is ill-posed as the number of unknowns, which are the polynomial moments of v, is bigger than the size of the system. The minimization has a sense only if $N_q > P$: we will suppose it is the case in the rest of the paper.

We use the abreviations sG-gPC$_P$ for the stochastic Galerkin gPC method with an expansion of the classical variable up to the order P and IPMM$_P - s - u_- u_+$ for the Intrusive Polynomial Moment Method with the entropy s with an expansion of the entropic variable up to order P. For example, IPMM$_5 - s_2 - 0.5 - 12.5$ corresponds to the solution obtained with the IPMM, with a polynomial expansion of the entropic variable of order 5; besides, the entropic variable is defined through $s_2(u) = -\ln(u - u_-) - \ln(u_+ - u) = -\ln(u - 0.5) - \ln(12.5 - u)$.

3.3.2. IC$_1$ test-case

This test-case has continuous initial conditions. The initial profile of the IC$_1$ test-case is given Fig. 3 (left), for one realization of the uncertain parameter ξ. It consists of three different states, translated by $\sigma\xi$ on the x-axis: $u(x, 0, \xi) = u^0(x + \sigma\xi)$. Fig. 4 (top right) shows the initial conditions for several realizations of ξ; the smooth curve is the mean of u at $t = 0$. For a specific realization, see Fig. 4 (top left), as t increases, the left state moves toward increasing x and the intermediate slope is steepening until the formation of a discontinuity at $t^* = -\frac{x_1 - x_0}{K_1 - K_0} = 1/11$ and $x^* = x_1 = 1.5$. On Fig. 4 (bottom left) we show the time evolution of the mean and standard deviation until $t = T_f = 0.0909 \approx t^*$. On Fig. 4 (bottom
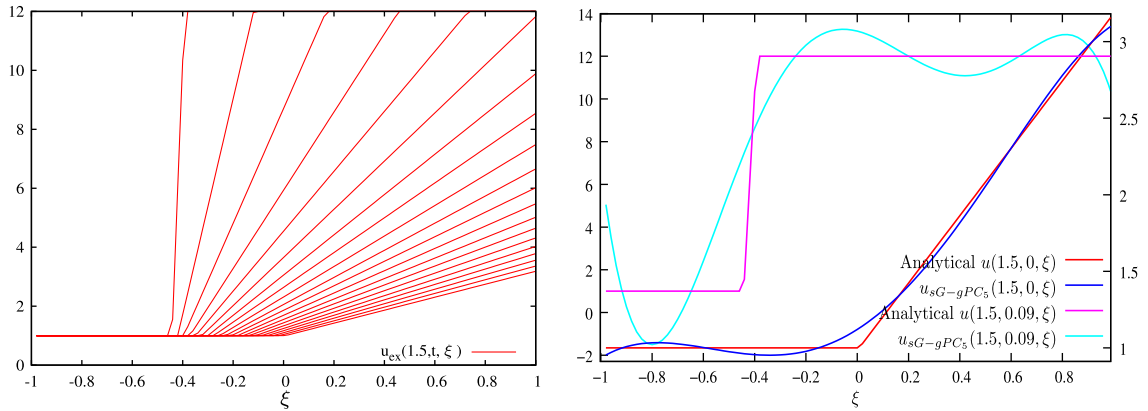
Fig. 6. Left: time evolution of the analytical solution at $x^* = 1.5$ vs. the random parameter ξ. Right: comparison between the analytical solution and the sG-gPC$_5$ solution at $t = 0$ and $t \approx t^*$ for $x^* = 1.5$. Initially, the oscillations are small but as time increases, the slope of the solution steepens leading to an aggravation of the Gibbs phenomenon and to possible numerical problems similar to those occuring in example 1 (note that the left scale is for $t \approx t^*$ and the right one for $t = 0$).
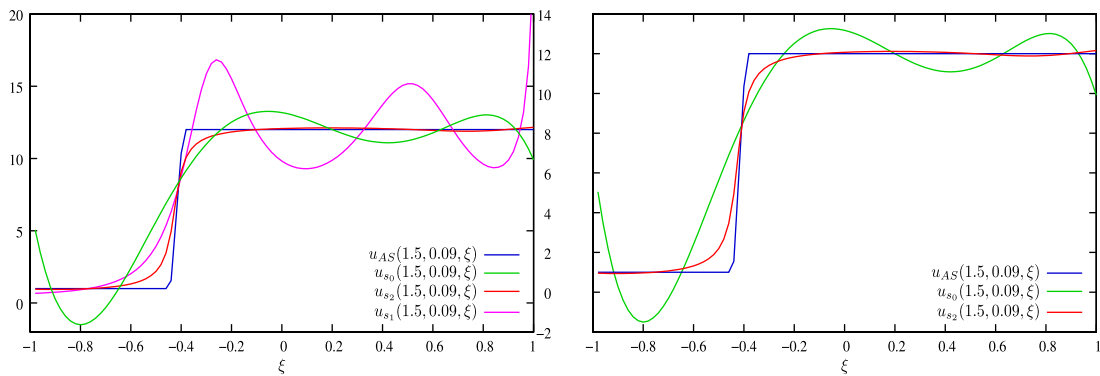
Fig. 7. Left: analytical solution, IPMM$_5 - s_0$, IPMM$_5 - s_1 - 0.5$ and IPMM$_5 - s_2 - 0.5 - 12.5$ at $x^* = 1.5$ and $T_f = 0.09 \approx t^*$. Right: Comparison between the analytical solution, sG-gPC$_5$ solution and IPMM$_5 - s_2 - 0.5 - 12.5$. Both pictures show solutions at $t = T_f = 0.0909 \approx t^*$ and $x^* = 1.5$ with respect to ξ. The number of grid cells is 100.

and for some values of ξ, u falls far below the zero-level. This has no physical implication in the Burgers' equation. However it can become a hassle for the stochastic Euler equations for example, for which a negative internal energy questions the hyperbolicity of the system or for which a negative density would not be physical.

Let's now consider the results from the IPMM and compare them to the results from the sG-gPC. Fig. 7 shows the results for $P = 5$[6] at $x^* = 1.5$ and $t = t^*$ for the entropies s_0, s_1 and s_2 given in (19). The entropy s_0 is such that the entropic variable is equal to the classical variable: developing the entropic variable onto the polynomial basis is then equivalent to develop the classical one onto the polynomial basis and consequently, the IPMM$_P - s_0$ is equivalent to the sG-gPC$_P$ (see the "$u_{s_0}(1.5, 0.09, \xi)$" curve on Fig. 7). Let us consider the entropy s_1 (20): the definition implies that u is constrained to $]u_-, +\infty[$.[7] On Fig. 7,[8] the oscillations of the s_1-curve are controlled near u_- but are not controlled in the upper part of the domain. For the entropy s_2, the definition domain of u is $]u_-, u_+[$ so that the oscillations are controlled on both bounds of the random domain, see the "$u_{s_1}(1.5, 0.09, \xi)$" curve on Fig. 7. Some oscillations still exist but they are forced to remain within the definition domain by construction, see Fig. 7 (right).

Fig. 8 shows how the expansion order P affects the solution with respect to ξ for sG-gPC$_P$ and for IPMM$_P - s_2 - 0.5 - 12.5$: low polynomial orders for the IPMM$_P - s_2 - 0.5 - 12.5$ already enable the solution testifying of the steep dependencies with respect to ξ whereas it is not the case for sG-gPC$_P$ with $P \leqslant 3$. Besides, the oscillations are always constrained to the domain $]u_-, u_+[(=]0.5, 12.5[$ for this example). Let us recall that Burgers' equation satisfying a maximum principle, the choice of u_- and u_+ is done in function of the initial condition (see Remark 3.0.5): in our examples, we had to take $u_- < 1$ and $u_+ > 12$ as $\forall \xi \in [-1, 1], 1 \leqslant u(x, 0, \xi) \leqslant 12$.

---

[6] In 1D random dimension (IC_1 and IC_2 test-cases), $P = M$.

[7] $]a, b[$ denotes the open interval whereas (a, b) denotes the couple.

[8] The parameters u_- and u_+, for every following figures concerning Burgers' equation are chosen having Remark 3.0.5 in mind.
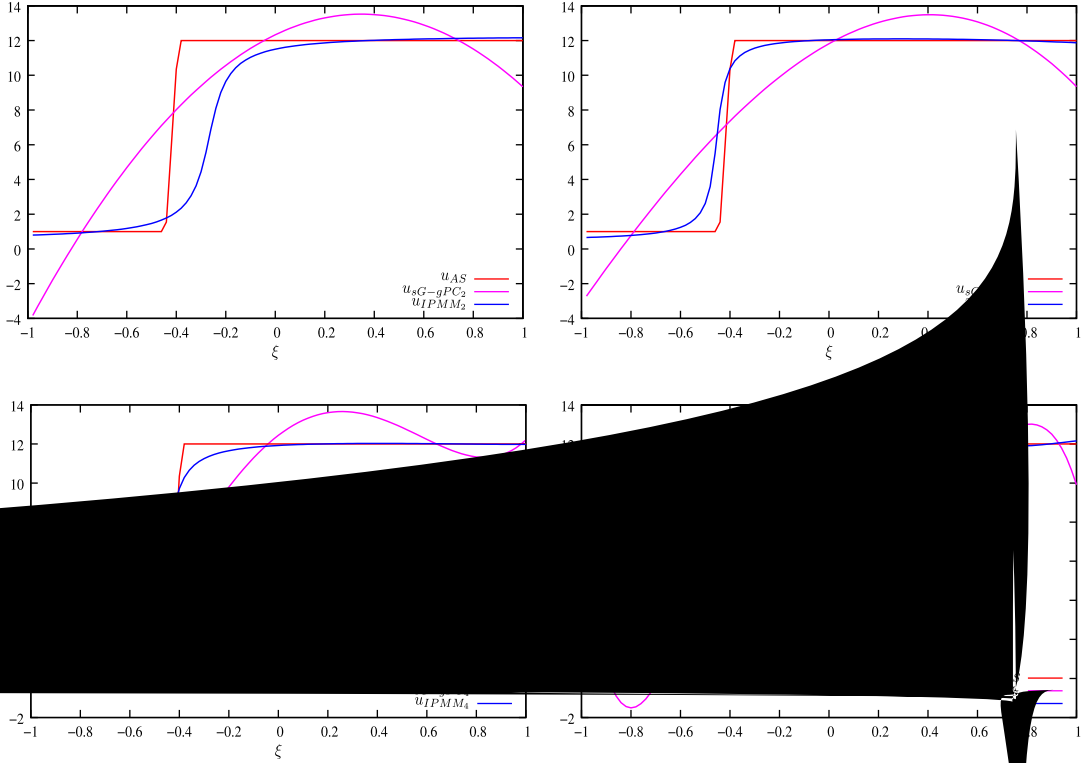
In order to interpretate more quantitatively these results, we consider the IC_2 test-case in the n... ...ion to perform some convergence test with respect to the polynomial order P for several values of the parameters u... ... . We will also compare the CPU times for both methods.

3.3.3. IC_2 test-case and convergence tests

The IC_2 initial condition is similar to the IC_1 but instead of an affine section between $x_0 + \sigma\xi$ and x... ... it has a polynomial part of order 3. Despite the smooth nature of the solution and its derivatives for a finite time, t... ...blem is still a numerically hard test-case as it exhibits very steep dependencies with respect to ξ at the space location... ...4 and at time $t = 0.06$: this can be seen in Fig. 9 (left) where the sG-gPC$_5$ and the IPMM$_5$ are compared. One can see t... ...polynomial of order 5 (sG-gPC$_5$) is not enough to approximate the solution and neither a polynomial of order 10 (see Fig... ...ht). We compare the performances of both method on this test case. All the simulations have been performed on a In... ...Xeon(R) CPU 5150 @ 2.66 GHz. The CPU times were obtain with the 'time' command. We consider the relative error i... ...mean and the standard deviation taken over the whole physical space and the relative errors in the $L^1(\Omega)$ an... ...$\Omega)$-norms at $x = 1.4, t = 0.06$. Their expressions are for the sG-gPC and the IPMM are, respectively:

$$e_{sG-gPC}^{L^j}(x,t) = \frac{\int \left| u_{ex}(x,t,\xi) - \sum_{i=0}^{P} u_i(x,t)\phi_i(\xi) \right|^j \mathrm{d}_w\xi}{\int |u_{ex}(x,t,\xi)|^j \mathrm{d}_w\xi}, \quad j = 1,2$$

$$e_{IPMM}^{L^j}(x,t) = \frac{\int \left| u_{ex}(x,t,\xi) - u\left(\sum_{i=0}^{P} v_i(x,t)\phi_i(\xi)\right) \right|^j \mathrm{d}_w\xi}{\int |u_{ex}(x,t,\xi)|^j \mathrm{d}_w\xi}, \quad j = 1,2.$$

Fig. 10 shows that the IPMM$_P$ errors on the mean, the standard deviation, the $L^2(\Omega)$-norm and on the L... ...-norm are always lower than the sG-gPC$_P$ errors for all P from 1 to 27 for three spatial discretizations (500, 1000 and ...00 cells). The figure also shows that IPMM presents a spectral convergence with respect to P for early polynomial orde... for 500 cells, the spectral convergence occurs up to $P = 4$, for 1000 cells up to $P = 5$ and for 2000 cells up to $P = 7$ i.e. re... ng the spatial domain ensures spectral convergence up to higher polynomial orders. Besides, for higher polynomial order... e errors have the same asymptotic behaviors: the limits depend only on the spatial discretizations and are the same for s... PC and IPMM. IPMM shows a faster convergence to this limit. Fig. 10 (bottom left) compares the convergence tests... sG-gPC$_P$ and IPMM$_P - s_2$ for several values of the pair (u_-, u_+): the closer is the pair to the analytical solution's extremal... ues, the more
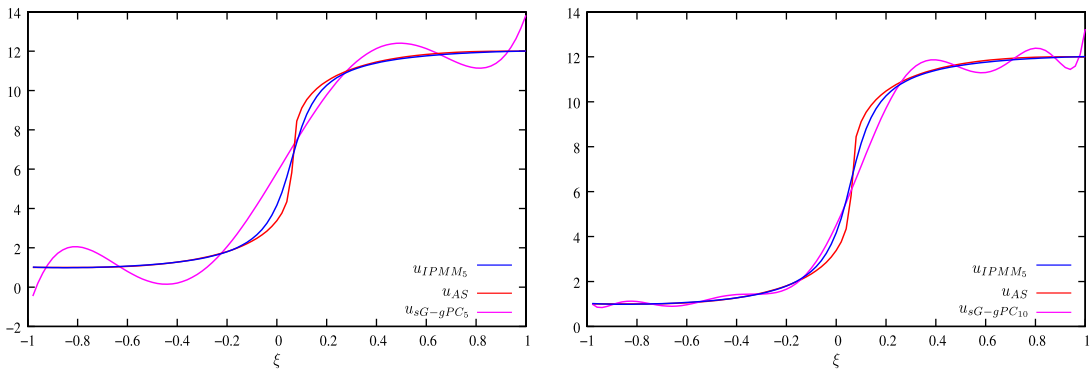
Fig. 9. Left: comparison between analytical solution, sG-gPC$_5$ and IPMM$_5 - s_2 - 0.5 - 12.5$ for IC_2 at $T_f = 0.06, x^* = 1.4$. Right: comparison between sG-gPC$_{10}$, IPMM$_5 - s_2 - 0.5 - 12.5$ in the same conditions.

accurate is the solution. In practice, we have noticed that if u_- and u_+ are too close to the extremal values of the analytical solution, the problem of the minimization of the entropy is ill-posed. One remedy is to increase the polynomial order (see Remark 2.3.3). For example, taking $(u_-, u_+) = (0.9, 12.1)$ and $P = 5$ is not enough to have an α-convex Legendre transformation of the entropy: the minimization algorithm does not converge as the constraints are too strong for this low polynomial order. In this case, increasing the order up to $P = 6$ is enough to solve the problem.

Fig. 10 (bottom right) compares the logarithm of the computational times for both methods (sG-gPC vs. IPMM $- s_2 - 0.5 - 12.5$) for the precedent discretizations. IPMM is more time consuming than sG-gPC: it needs a minimization operation in addition to the classical sG-gPC steps. The growth of the computational cost with respect to the polynomial order P is the same for both methods (the slopes of the curves are the same). According to Fig. 10, the computational time for both methods takes the form $t_{CPU}^{sG-gPC} \approx b(N_x)e^{\alpha P}$ and $t_{CPU}^{IPMM} \approx \beta(N_x)e^{\alpha P}$ where N_x is the number of the cells and $b(Nx) < \beta(N_x)$. Nevertheless, IPMM remains interesting: Table 1 compares (for a given accuracy on the mean) the polynomial order, the accuracy on the standard deviation, the CPU time and the error in $L^1(\Omega)$ and $L^2(\Omega)$-norm of both methods. IPMM is superior based on theses criterions: note that it also ensures the solution to remain in the bounds defined by u_- and u_+. Besides, for a given accuracy, IPMM needs a lower truncation order which is directly linked with the memory requirements: this is encouraging for higher stochastic dimension problems for which the number of polynomial moments grows exponentially fast.

It is possible to reduce the amount of work by performing a local IPMM, and thus minimizing the Legendre transform of the entropy only in the vicinity of the discontinuities. This would imply the introduction of heuristics so as to decide where the minimization is applied or not, which we do not want in this paper.

4. Burgers' equation in 2-D random dimension

We consider one 2-D initial condition which is representative of multiple shock flows encountered in compressible fluid mechanics. Again, we refer to Appendix A for more quantitative details about the initial conditions and their respective analytical expressions.

This 2-D test-case IC_3 emphasizes several issues encountered for example in ICF flows. In this case, one wants to maximise the compression rate of a fluid so that it reaches required temperature and pressure for ignition at one specific location. A succession of multiple little shocks is preferable to be close to the isentropic limit (otherwise, in the case of a perfect gas, the maximum compression is limited to $\frac{\gamma+1}{\gamma-1}$). The IC_3 test-case tackles the issue of a succession of two shocks with uncertain left states, see Fig. 11 (left). In the space of the uncertain parameters, the solution presents two or three different states depending on the position and time of interest. In the following, we will compare response surfaces from sG-gPC and IPMM solutions to the analytical solution, at different times and space locations. Figs.12–14 come from the same computation at different times and space locations.

Let us describe more precisely the test-case: initially, it consists of two shocks with uncertain left states. As t increases, the first shock reaches the second one to form a unique shock at time $t^* = 0.055$, see Fig. 11 (right) for the time evolution of the solution for one realization of the random variables. This capture always happens whatever the realizations of the uncertain parameters are, as $\overline{K_0} + \sigma_0\xi_0 > \overline{K_1} + \sigma_1\xi_1 \forall (\xi_0, \xi_1) \in [-1, 1] \times [-1, 1]$. The standard deviation (not presented) grows at the shock position as time increases. As time tends to t^*, the analytical solution in the random space consists of three affine states, see for example the top pictures of Figs. 12 and 13 or Appendix A.

Remark 4.0.1. The test case can be made stiffer by changing the values of σ_0 and σ_1 to increase the slope $\frac{\sigma_0}{\sigma_1}$ of the oblique shock in the (ξ_0, ξ_1)-space, see Fig. 12 and Appendix A.

The oblique shock, the fastest one, reaches the second one and overtakes it at time $t^* = 0.055$, see Fig. 13 (top-right picture).
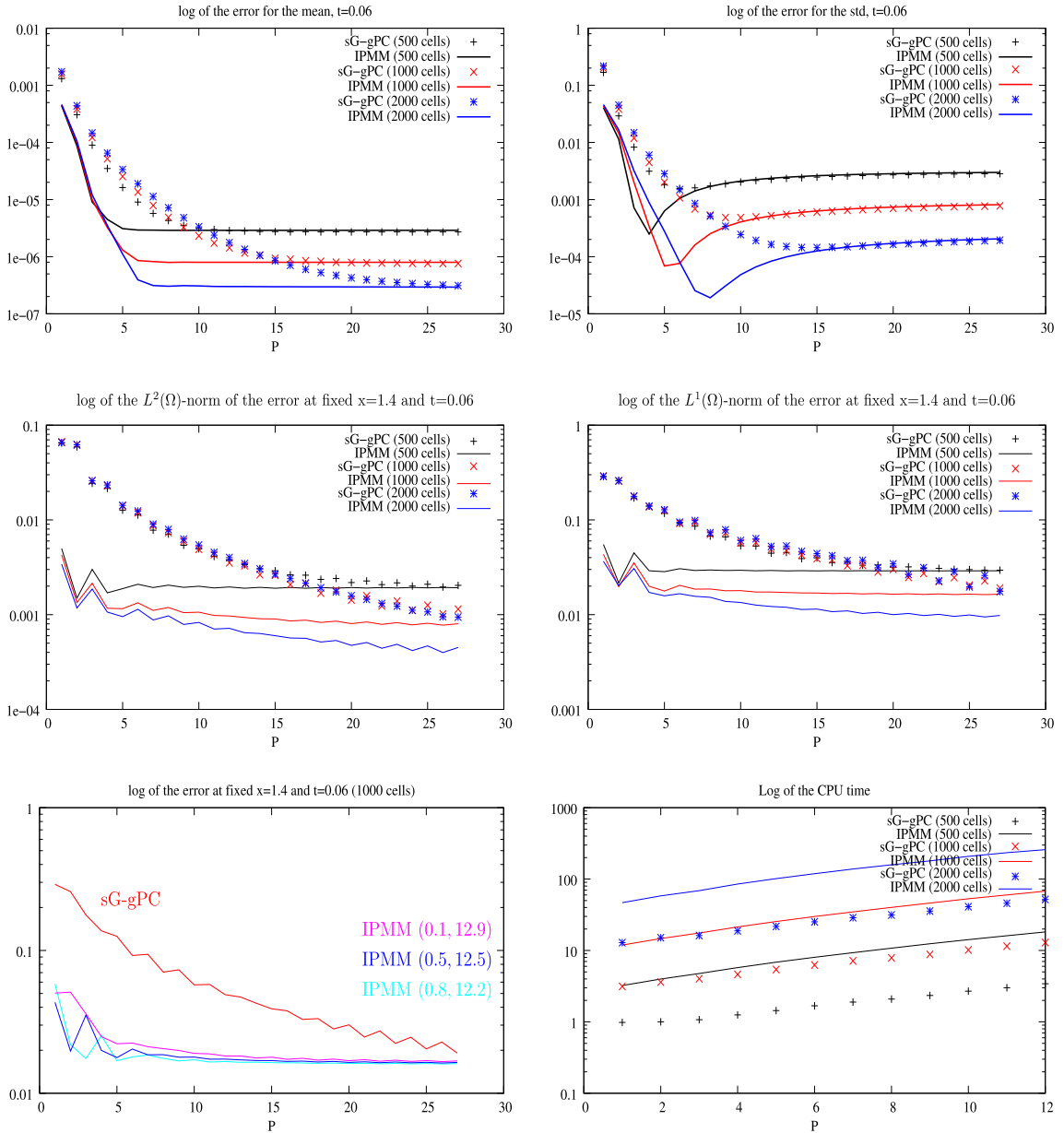
Fig. 10. Comparison between sG-gPC$_P$ and IPMM$_P$ for several spatial discretizations (500, 1000 and 2000 cells) and several polynomial orders P, semi-logarithmic scale. Top: convergence tests at $t = 0.06$ for IC_2 for the mean (left) and the standard deviation (right) taken over the whole x-space. Middle: convergence tests at $t = 0.06$ and $x^* = 1.4$ for IC_2 with respect to the polynomial order $P, L^2(\Omega)$-norm of the error (left) and $L^1(\Omega)$-norm of the error (right). Bottom left: comparison between sG-gPC$_P$, IPMM$_P - s_2 - 0.1 - 12.9$, IPMM$_P - s_2 - 0.5 - 12.5$ and IPMM$_P - s_2 - 0.8 - 12.2$. Bottom right: CPU times with respect to the polynomial order P. IPMM is more time consuming than sG-gPC (as it needs one more computational step: the minimization algorithm). The rate of increase of the CPU times is the same for both methods.

Table 1
For a 2000 cells spatial discretization and a given accuracy on the mean, IPMM$_7$ is about 7 times more accurate on the standard deviation, 1.7 times more accurate in $L^2(\Omega)$-norm, 1.6 times more accurate in $L^2(\Omega)$-norm, 3.5 times faster, and needs 3.5 times less polynomial coefficients than sG-gPC$_{27}$.

	Given accuracy for the mean	Acc. for the std	CPU time	Acc $L^2(\Omega)$-norm	Acc. $L^1(\Omega)$-norm	$P+1$
IPMM$_7$ (2000 cells)	3.1205×10^{-7}	2.541×10^{-5}	2 min 15 s	5.3407×10^{-4}	1.06077×10^{-2}	8
sG-gPC$_{27}$ (2000 cells)	3.1128×10^{-7}	1.936×10^{-4}	7 min 18 s	9.4370×10^{-4}	1.75344×10^{-2}	28
Ratio (sG-gPC/IPMM)	$0.9975 \approx 1$	7.62	3.5	1.76	1.652	3.5
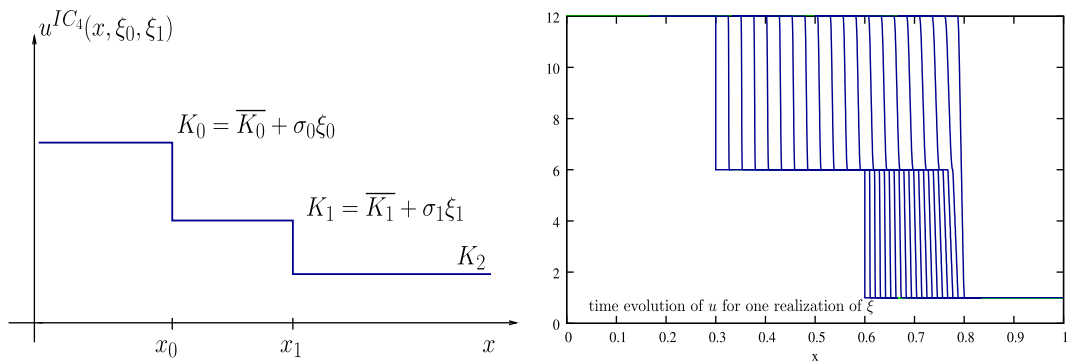
Fig. 11. Initializations for test-case IC_3 (left) and time evolution of the solution for one realization of the random variables: the second shock reaches the first one whatever the realization of the random variables and absorbs is (right).

Let's now compare solutions from sG-gPC and IPMM in the random space. In the following, the solution is computed with 6000 cells (for both sG-gPC and IPMM), $CFL = 0.5$ and the polynomial order is 4–4; besides, for the IPMM, the entropy is s_2 and the pair (u_-, u_+) is (0,12.5).

Fig. 12 shows the analytical solutions (top pictures), the sG-gPC solutions (middle pictures) and the IPMM solutions (bottom pictures) at time $t = 0.0538$ and position $x = 0.785$ (left column) and at time $t = 0.054$ and position $x = 0.785$ (right column). On the left column (middle), the solution from sG-gPC have important oscillations whereas the solution from IPMM is more stable (bottom). Besides, the sG-gPC solution does not capture the intermediate state (state $u = 6$ for the analytical solution) whereas the state is clearly identifiable for the IPMM solution at the bottom left of Fig. 12. The intermediate state is captured but some oscillations are generated in its vicinity. This is because IPMM controls oscillations at the bounds of the domain of u but not within this domain. Moreover, the fluctuating scales are not the same for both methods: the sG-gPC solution is going far below the 0-bound and the 12.5-bound as one can see on Figs. 12 and 13.

The results at time $t = 0.0545$ are given for $x = 0.791$ on Fig. 13 (left column). At this time and position, the intermediate state is even harder to capture. The sG-gPC solution fails whereas the IPMM captures it. Besides, as the solution starts having steeper dependencies with respect to the uncertain parameters, the amplitude of the oscillations for sG-gPC are more important than on the previous figures. The phenomenon is even aggravated on Fig. 13 (right column) for the final time for which the analytical solution consists in one steep and oblique discontinuity with respect to the uncertain parameters.

These 2D simulations are performed using 6000 cells, a 4–4 polynomial order implying the computation of 25×25 matrix in the minimization algorithm and a full 2D quadrature points grids (tensorised level 3 in the 1D Clenshaw–Curtis rule). Note that in higher stochastic dimension, the calculation could be optimized by using sparse grids or adaptative sparse grids for the numerical integration, see [38,13,10]. The "curse of dimensionality", i.e. the explosion of the amount of work with the dimension, is of course an important issue in UQ but we do not tackle it in this paper.

The last set of figures of this section concerns an early time in the preceding simulation: at $t = 0.01115$ when the shocks are not close enough to interact with each other. Fig. 14 (top left) shows the analytical solution for the slowest shock whereas Fig. 14 (top right) shows the analytical solution for the oblique shock. The figures show, respectively, a discontinuity between the lower state and the intermediate state and a discontinuity between the intermediate state and the upper one. As the IPMM is not designed to control oscillations within the domain defined by the pair (u_-, u_+), but only at its bounds, oscillations are not constrained in the vicinity of the intermediate state. On Fig. 14 (bottom left), we notice that the oscillations are controlled at the lower bound u_- but not close to the intermediate state. This explains what appears as a failure of IPMM. For the oblique shock, Fig. 14 (bottom right), the phenomenon is less visible and the result is still satisfying in comparison to the one obtained with sG-gPC (Fig. 14 (middle right)).

Several tracks have been investigated in order to control the oscillations within the bounds defined by the entropy but this will not be part of this paper. We considered, for example, the possibility of defining several entropies depending on the space location of the discontinuities, in agreement with a global entropy over the whole domain.

From these results, we conclude that the discontinuity locations for the IPMM are close to the analytical ones, even for the early time simulations for which the shocks are more spread out (Fig. 14).

5. Compressible gas dynamics

We have presented a new method based on analogies between UQ and Kinetic theory [7,30] and illustrated the different results on the simple example of the Burgers' equation. In this section, we present our first results in compressible fluid dynamics, making use of the ideas developed precedently. We also come back to the problem of example 1 – Fig. 1 of the introduction for which sG-gPC fails due to the appearance of Gibbs phenomenon giving birth to a negative mass density (see Remark 5.2.1 for more details). We refer to [21] for a study of a similar physical framework.
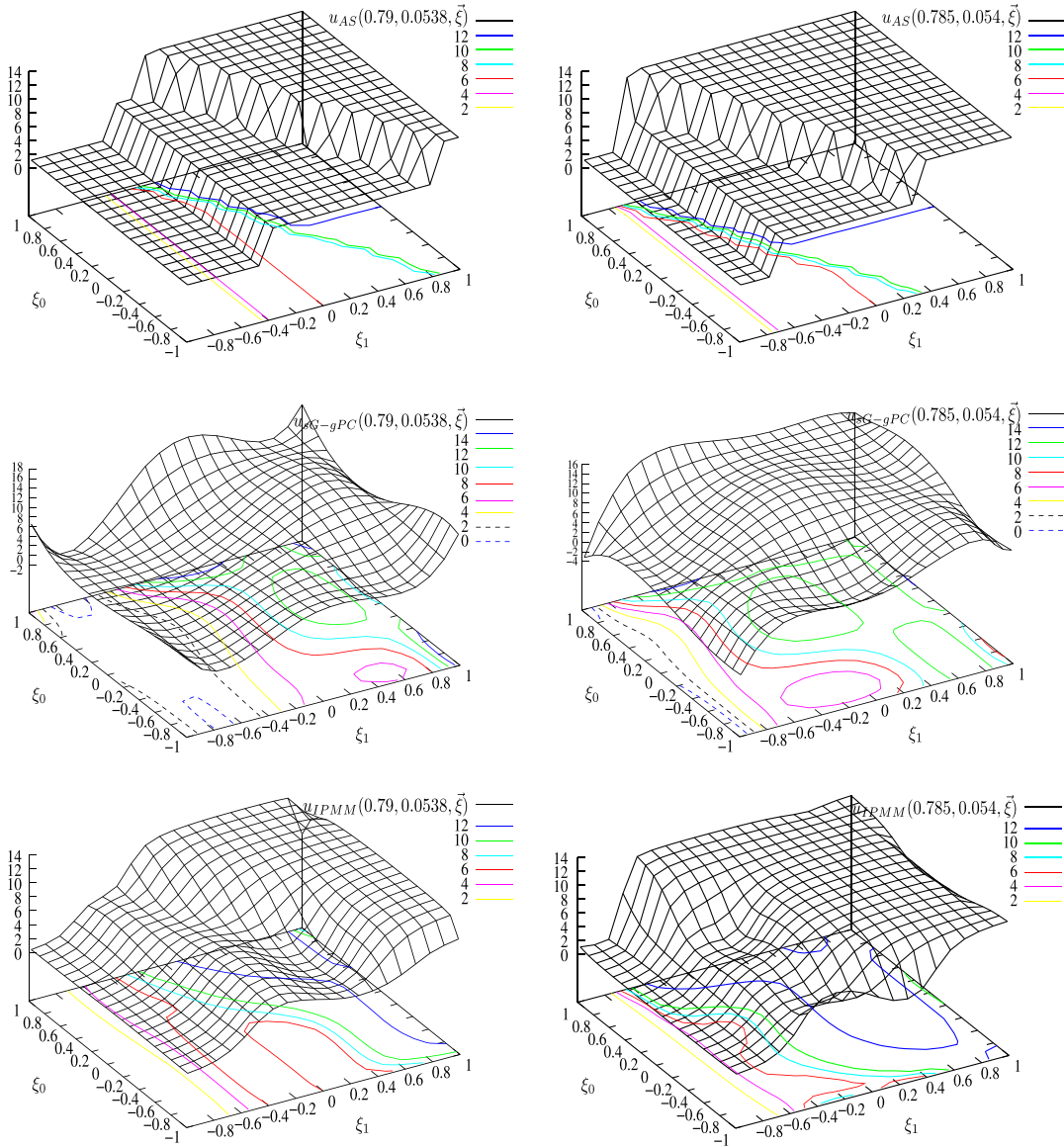
Fig. 12. Results at time $t = 0.0538$ and position $x = 0.79$ (left column) and at time $t = 0.054$ and position $x = 0.785$ (right column). Analytical solution (top), sG-gPC (middle), IPMM (bottom). The IPMM solution is more accurate than the sG-gPC solution. The scales are different on the pictures: on the sG-gPC figure, oscillations are not controlled, the solution goes above the upper state and beneath the lower one. The discontinuities are well located for the IPMM solution, this is characteristic of conservative schemes.

5.1. Euler system, entropy and entropic variable

The Euler system for compressible fluid mechanics in 1D cartesian coordinate is

$$
\begin{cases}
\partial_t \rho + \partial_x \rho u = 0, \\
\partial_t \rho u + \partial_x(\rho u^2 + p) = 0, \\
\partial_t \rho e + \partial_x(\rho u e + p u) = 0,
\end{cases}
\tag{25}
$$

where ρ is the density, u is the velocity, e is the total specific energy and p is the pressure. The system is closed by an equation of state for perfect gases $p = (\gamma - 1)\rho\epsilon$ where $\epsilon = e - \frac{u^2}{2}$ is the specific internal energy. This system is hyperbolic. It exists an entropy–entropy flux couple (s, g). Note that we can derive different entropy–entropy couple from (s, g): in the case of a

perfect gas.[9] if $h : x \to h(x)$ is such that $h'(x) \leqslant 0$ and $\gamma h''(x) + h'(x) \geqslant 0$, then $\tilde{s}(\rho, \rho u, \rho e) = -\rho h(s(\rho, \rho u, \rho e))$ is also an e
py for the system, see [34] (pp. 99–100 and pp. 161–162). Different entropies can have different behaviors as can be seen
Section 3 but in this paper, we will focus on the entropy–entropy flux couple defined by $s(\rho, \rho u, \rho e) = -\rho \ln(\rho^{-\gamma} \left(\rho e - \frac{(\rho u)^2}{2\rho} \right)$
and $g(\rho, \rho u, \rho e) = \frac{\rho u}{\rho} s(\rho, \rho u, \rho e)$. This entropy is such that the mathematical entropy s is the opposite of the physical entropy.

Let's denote by $U = (\rho, \rho u, \rho e)^t$ our vector of unknown. The entropic variable V, relative to s is

$$
V = \nabla_U s(U) = \begin{pmatrix} v_1 \\ v_2 \\ v_3 \end{pmatrix} = \begin{pmatrix} -\ln \left(\frac{2(\rho e)\rho - (\rho u)^2}{2\rho^{\gamma+1}} \right) + \gamma + \frac{-(\rho u)^2}{2\rho(\rho e) - (\rho u)^2} \\ \frac{2\rho(\rho u)}{2\rho(\rho e) - (\rho u)^2} \\ -\frac{2\rho^2}{2\rho(\rho e) - (\rho u)^2} \end{pmatrix}, \tag{26}
$$
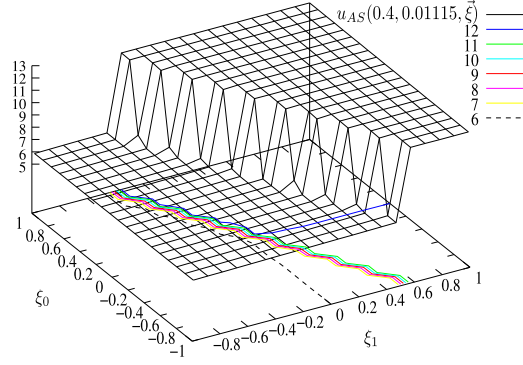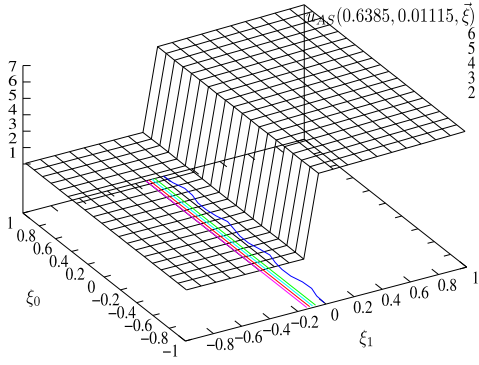
and the bijection $V :\to U(V)$ is given by

$$U(V) = \begin{pmatrix} \rho \\ \rho u \\ \rho e \end{pmatrix} = \begin{pmatrix} e^{\frac{2v_1 v_3 - 2v_3 \ln(-v_3) - 2v_3\gamma - v_2^2}{2v_3(\gamma-1)}} \\ -\frac{v_2}{v_3} e^{\frac{2v_1 v_3 - 2v_3 \ln(-v_3) - 2v_3\gamma - v_2^2}{2v_3(\gamma-1)}} \\ \frac{v_2^2 - 2v_3}{2v_3^2} e^{\frac{2v_1 v_3 - 2v_3 \ln(-v_3) - 2v_3\gamma - v_2^2}{2v_3(\gamma-1)}} \end{pmatrix}. \tag{27}$$

Remark 5.1.1. Even once V is developed on the polynomial basis, the method ensures the positiveness of the mass density: this is explicit in (27) where the expression of ρ with respect to V has an exponential form.

The next step concerns the development of V on the P-truncated polynomial basis, $V = \sum_{k=0}^{P} V_k \phi_k$, and the resolution of the P-truncated system of conservation law

$$\partial_t \begin{pmatrix} \int U\left(\sum_{i=0}^{P} V_i \phi_i\right) \phi_0 \mathrm{d}w \\ \cdots \\ \int U\left(\sum_{i=0}^{P} V_i \phi_i\right) \phi_P \mathrm{d}w \end{pmatrix} + \partial_x \begin{pmatrix} \int f\left(U\left(\sum_{i=0}^{P} V_i \phi_i\right)\right) \phi_0 \mathrm{d}w \\ \cdots \\ \int f\left(U\left(\sum_{i=0}^{P} V_i \phi_i\right)\right) \phi_P \mathrm{d}w \end{pmatrix} = 0, \tag{28}$$

where $f(U) = f(\rho, \rho u, \rho e) = \begin{pmatrix} \rho u \\ \frac{(\rho u)^2}{\rho} + (\gamma - 1)\left(\rho e - \frac{1}{2} \frac{(\rho u)^2}{\rho}\right) \\ \frac{(\rho u)(\rho e)}{\rho} + (\gamma - 1) \frac{\rho u}{\rho}\left(\rho e - \frac{1}{2} \frac{(\rho u)^2}{\rho}\right) \end{pmatrix}$, using the equation of state.

5.2. Numerical discretization

We define $\int V \phi_t \mathrm{d}w = V_t$, $\int U\left(\sum_{k=0}^{P} V_k \phi_k\right) \phi_t \mathrm{d}w = U_t$ and $\int f\left(U\left(\sum_{k=0}^{P} V_k \phi_k\right)\right) \phi_t \mathrm{d}w = f_t$, so that (28) can be written

$$\partial_t \begin{pmatrix} U_0 \\ \cdots \\ U_P \end{pmatrix} + \partial_x \begin{pmatrix} f_0 \\ \cdots \\ f_P \end{pmatrix} = 0, \tag{29}$$

and we integrate in space over a cell and in time over a time step (Finite Volume (FV) formulation)

$$\frac{1}{\Delta t} \begin{pmatrix} U_{0,j}^{n+1} - U_{0,j}^{n} \\ \cdots \\ U_{P,j}^{n+1} - U_{P,j}^{n} \end{pmatrix} + \frac{1}{\Delta x_j} \begin{pmatrix} f_{0,j+1/2}^* - f_{0,j-1/2}^* \\ \cdots \\ f_{P,j+1/2}^* - f_{P,j-1/2}^* \end{pmatrix} = 0, \tag{30}$$

where $f_{k,j+1/2}^* = \frac{1}{\Delta t} \int_{t^n}^{t^{n+1}} \left(\int f\left(U\left(\sum_{i=0}^{P} V_i(x_{j+1/2}, t) \phi_i(\xi)\right)\right) \phi_k(\xi) \mathrm{d}_w \xi\right) \mathrm{d}t$. We commute the FV formulation and the integrals with respect to ξ

$$f_{k,j+1/2}^* = \int \left(\frac{1}{\Delta t} \int_{t^n}^{t^{n+1}} f\left(U\left(\sum_{i=0}^{P} V_i(x_{j+1/2}, t) \phi_i(\xi)\right)\right) \mathrm{d}t\right) \phi_k(\xi) \mathrm{d}_w \xi,$$

$$f_{k,j+1/2}^* = \int f_{j+1/2}^*(\xi) \phi_k(\xi) \mathrm{d}_w \xi.$$

The discretized system is

$$\frac{1}{\Delta t} \begin{pmatrix} U_{0,j}^{n+1} - U_{0,j}^{n} \\ \cdots \\ U_{P,j}^{n+1} - U_{P,j}^{n} \end{pmatrix} + \frac{1}{\Delta x_j} \begin{pmatrix} \int f_{j+1/2}^* \phi_0 \mathrm{d}w - \int f_{j-1/2}^* \phi_0 \mathrm{d}w \\ \cdots \\ \int f_{j+1/2}^* \phi_P \mathrm{d}w - \int f_{j-1/2}^* \phi_P \mathrm{d}w \end{pmatrix} = 0. \tag{31}$$

The integrals are evaluated using numerical quadratures. This enables one to have the choice in the numerical scheme: in our case, $(f_{j+1/2}^*(\xi_l))_{l \in \{1,\dots,N\}}$ (the flux evaluated at the quadrature points) are computed using a high-order Lagrange + Remap FV scheme based on the well known Godunov acoustic Riemann solver. We do not give further details about the numerical scheme as it is not the purpose of this paper, for more details, see for example [15].

Remark 5.2.1. The same kind of approach as been used for the discretization of sG-gPC for the example 1 – Fig. 1. The only difference comes from the definition of the fluxes:

$$f_{k,j+1/2}^* = \int \left(\frac{1}{\Delta t} \int_{t^n}^{t^{n+1}} f\left(\sum_{i=0}^{P} U_i(x_{j+1/2}, t) \phi_i(\xi)\right) \mathrm{d}t\right) \phi_k(\xi) \mathrm{d}_w \xi = f_{k,j+1/2}^* = \int f_{j+1/2}^*(\xi) \phi_k(\xi) \mathrm{d}_w \xi.$$

The integrals being evaluated using numerical quadratures and the fluxes, taken at the quadrature points, computed with the same numerical scheme as IPMM. This scheme needs the definition of the sound speed $c = \sqrt{\gamma p / \rho}$ in each cell for the construction of the flux: in the uncertain Sod test case of example 1, the solution presents stiff dependences with respect to ξ and there exists at least one ξ_m such that $\rho_j^n(\xi_m) = \sum_{k=0}^{P} \rho_{k,j}^n \phi_k(\xi_m) < 0$ leading to a negative product under the square root in the expression of c. This is why sG-gPC crashes at the first time step.

5.3. Numerical results

Let's consider the problem presented in example 1 – Fig. 1, an uncertain Sod test case with uncertainty carried on the initial interface position between a light fluid and a heavy fluid. We take $\gamma = 1.4$ and the initial conditions are

$$\begin{cases} \rho(x,0,\xi) = \begin{cases} 1 & \text{if } x \leqslant x_{\text{interface}}(\xi) \\ 0.125 & \text{otherwise} \end{cases}, \\ \rho u(x,0,\xi) = 0, \\ \rho e(x,0,\xi) = \begin{cases} 2.5 & \text{if } x \leqslant x_{\text{interface}}(\xi) \\ 0.25 & \text{otherwise}. \end{cases} \end{cases}$$

The uncertainty is injected at the interface position $x_{\text{interface}}(\xi) = 0.5 + 0.05\xi$ where $\xi \in [-1, 1]$ parametrizes a uniform law. For one realization of the random variable, we recall that the solution consists of a shock wave, propagating in the *light fluid* (right side of the interface), a contact discontinuity and a rarefaction wave in the *heavy fluid*. Fig. 15 shows results (mean and standard deviation of the density, spatial distributions) obtained with the IPMM in Eulerian coordinates. Table 2 gives the CPU time and the percentage of the total work devoted to the minimization algorithm for the resolution of the uncertain Sod shock tube for different truncation orders. Note that every computation lasts less than one minute.

We remind the reader that sG-gPC fails on this test case: the oscillations occuring initially were leading to a negative mass density for several quadrature points and the numerical scheme considered can not deal with such difficulties (the calculations of $(f_{j+1/2}^*(\xi_l))_{l \in \{1,\dots,N\}}$ needs positive realizations of the mass density, see Remark 5.2.1 for more details).

The simulation has 200 cells, uses a 3rd order Lagrange + Remap scheme based on the acoustic solver (see [15]) and the polynomial development is carried out up to order 11. One advantage of the method is the possibility of using high-order schemes that provides converged results with less grid points, consequently reducing the cost (see Table 2 for the computational costs).

Fig. 15 (right) shows the mean and the standard deviation of the mass density at time $t = 0.14$, obtained with $IPMM_{11}$ and by integration of analytical formulae (see [37]). The results show a good agreement with the analytical solution, the position of the three waves are corresponding and the amplitude of the standard deviation is quite well captured (except for the rarefaction fan's: this difficulty is a typical issue in the study of deterministic solvers, see [15]). Fig. 15 (left) shows the time evolution of the mean and standard deviation of the mass density, the initial conditions being those of example 1 – Fig. 1. The possible locations of the three sharp fronts corresponding, from left to right, to a rarefaction fan, a contact discontinuity and a shock wave coincide with regions of large standard deviation and varying mean values. It is interesting to see how these spatial distributions of uncertainty evolve in time. At early times, the whole uncertainty is mainly localized close to the center of the domain with a sharp peak. Later on, the three distinct regions appear and are more spaced out. Standard deviations are null and mean values are constant in between those regions. It is also interesting to see that the region of large standard deviation are advected similarly to the deterministic case. The uncertainty regions associated with the contact discontinuity and the shock are simply advected to the right. The distributions are symmetric and of similar amplitude. The uncertainty region associated with the shock is the fastest one and diffuses slightly more than the other one. Their advection velocities are unaffected by the random parameter. The behavior of the uncertainty region of the rarefaction fan is more
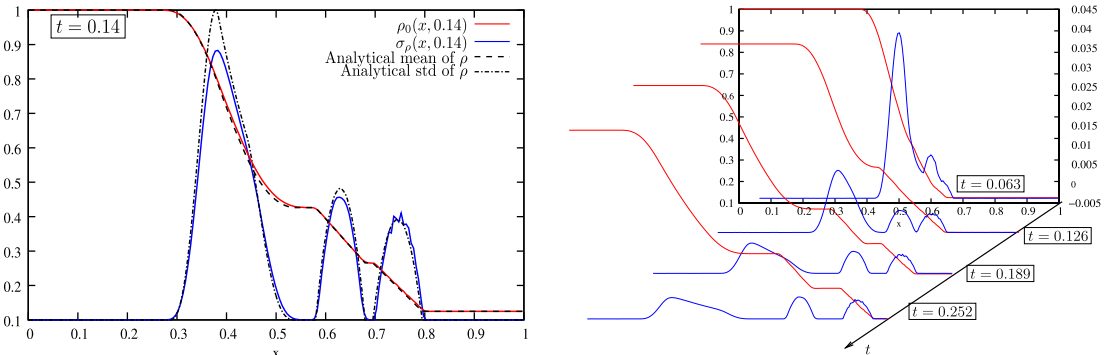

Fig. 15. Left: mean and standard deviation of the mass density at $t = 0.14$ using IPMM with 11th truncation order, a 3rd order Lagrange + Remap scheme based on the acoustic solver and 200 cells. The analytical solution are obtained by numerical integration of the analytical formulae [37]. The initial conditions are given Fig. 1. Right: time evolution of the mean and standard deviation of the mass density. Three waves carrying uncertainty are propagating: a rarefaction wave, a interface and a shock.

Table 2
CPU cost for different polynomial order on the uncertain Sod test case described in Section 5.3. Computations have been done on a Intel(R) Xeon(R) CPU 5150 @ 2.66 GHz CPU. The simulations have 200 cells. They all take less than one minute. The last line shows the evolution of the percentage of work dedicated to the minimization algorithm as the order of truncation P increases.

Polynomial order of IPMM	1	2	3	4	5	6	7	8	9	10	11
CPU time ($t \in [0, 0.14]$) (s)	17.62	18.47	19.74	21.46	23.20	25.67	27.78	30.45	33.56	36.17	40.51
% of CPU work for Newton algorithm	22.5	30.4	40.2	47.5	54.9	60.0	65.4	69.3	73.4	76.6	78.7

complex. Its large amount of uncertainty tends to diffuse to the left in an unsymmetrical fashion. This temporal change in the shape of the distribution is due to non-linear phenomena mainly related to the pressure term of the system (results not presented here).

6. Conclusion

In this paper we have described and applied a new method to propagate uncertainty in systems of conservation laws. The method is intrusive, conservative and based on both Kinetic theory and Polynomial Chaos theory, making a parallel between theory of moments and the polynomial moments of the solution. The main point is that the polynomial expansion is not carried out on the main variable but on its associated entropic variable defined through the entropy–entropy flux pair. It gives birth to a new hyperbolic system of conservation laws written in terms of bijection between both variables. Several theorical properties of this new system have been stated and can be directly derived from the analogy made with Kinetic theory [7,30] and PC approach. We have applied the Intrusive Polynomial Moment Method and the stochastic Galerkin gPC method on a relatively simple scalar equation: the stochastic inviscid Burgers' equation in one dimensional space. We have first illustrated the properties of the method on the one dimensional random problem. We have demonstrated the appearance of Gibbs phenomenon using the stochastic Galerkin gPC method; concerning this point, we used a Roe scheme to solve the system. We have then presented and compared both methods on a discontinuous test-case, putting forward how important is the choice of the entropy with respect to the domain invariant to control the oscillations. We have also performed some convergence tests on a stiff problem: the IPMM revealed to be more accurate than the sG-gPC for any polynomial orders, providing spectral convergence rates for the early polynomial orders (deteriorating with the grid size). For a given accuracy, the new approach reveals to be faster and less memory consuming, due to its fast convergence (better spectral convergence rates than sG-gPC), despite the costing minimization step it implies during the computations. Finally, we have used our method to solve one 2-D random dimension test-case, tackling important issues encountered for complex stochastic conservation laws. Once again, the new method has proved its efficiency by controlling oscillations at the bounds of the domain defined by the entropy and capturing steep dependencies with respect to the uncertain parameters (even for low polynomial orders).

For the Burgers' equation, *a priori* knowledge of the solution, as the equation satisfy a maximum principle, allows us to carefully tune the parameters u_- and u_+ involved in our entropy expression. This is not always possible as not every system of conservation laws satisfies such a property. In compressible gas dynamics, the bounds defined by the entropy are provided by the physics of the problem: the natural entropy enables the control of the oscillations in the vicinity of zero for the mass density and the internal energy.

In this work, the discontinuities in the random space are not treated adaptively as others do [26,28,41]. With our approach, we do not need to split the domain in several elements nor track the position of the discontinuity in the random space. Nevertheless, it is possible to couple our method with adaptive ones. The method, using a minimization algorithm in every cells at every time steps, is quite time consuming (in some of our simulations, the minimization algorithm takes more than 70% of the total amount of time of the run). Fortunately, the use of high-order schemes provides converged results with less grid cells and can considerably reduce the time of the simulations. This improvement is noticeable in our first results in compressible gas dynamics results. We are currently working on the reduction of the cost of the method. It is possible to perform the minimization steps only in the vicinity of the discontinuities, but this implies introducing heuristics. Furthermore, the use of sparse grids to perform the numerical integrations enables us to extend the method to high random dimensions.

In a last section, we have used our method to solve compressible gas dynamics problems in Eulerian coordinates. The IPMM enabled us to solve the hydrodynamical test-case considered whereas the stochastic Galerkin gPC method crashes due to the appearance of a negative mass density. The oscillations are controlled so that the physical quantities are constrained to their respective physical domains. Finally, we emphasize that the method can be applied to any hyperbolic system of conservation laws.

Appendix A. Initial conditions and analytical solutions

We consider Eq. (18): $\partial_t u + \partial_x \frac{u^2}{2} = 0$. The analytical solutions for the different initial conditions are calculated by the method of the characteristics.

A.1. 1D test-case IC_1

– Initially a piecewise linear function: $u^{IC_1}(x, \xi) : \mathcal{D} = [0, L] \times [-1, 1] \rightarrow$, such that

$$u^{IC_1}(x, \xi) = K_0 \cdot_{[0,x_0]}(x - \sigma\xi) + K_1 \cdot_{[x_1,L]}(x - \sigma\xi) + \left(\frac{K_1 - K_0}{x_1 - x_0}(x - \sigma\xi) + \frac{K_0 x_1 - K_1 x_0}{x_1 - x_0}\right) \cdot_{[x_0,x_1]}(x - \sigma\xi).$$

– The analytical solution is for $t < t^*$:

$$u(x,t,\xi) = \begin{cases} K_0 & \text{if } x - \sigma\xi - K_0 t < x_0 \\ \frac{a(x-\sigma\xi)+b}{at+1} & \text{if } x_0 \leqslant \frac{x-\sigma\xi-bt}{at+1} \leqslant x_1 \\ K_1 & \text{if } \frac{x-\sigma\xi-bt}{at+1} \geqslant x_1 \end{cases}. \tag{A.1}$$

– In practice, we take $L = 3, K_0 = 12, K_1 = 1, x_0 = 0.5, x_1 = 1.5$ and $\sigma = 0.2$ so that $\sigma\xi \in [-0.2, 0.2]$.

A.2. 1D test-case IC_2

– Initially we have $u^{IC_2}(x,\xi) : \mathcal{D} = [0,L] \times [-1,1] \rightarrow$, such that

$$u^{IC_2}(x,\xi) = K_0 \cdot {}_{[0,x_0]}(x - \sigma\xi) + K_1 \cdot {}_{[x_1,L]}(x - \sigma\xi) + Q(x - \sigma\xi) \cdot {}_{[x_0,x_1]}(x - \sigma\xi)$$

with

$$Q(x) = ax^3 + bx^2 + cx + d.$$

The coefficients satisfying

$$a = -2\frac{K_0 - K_1}{x_0^3 + 3x_0x_1^2 - x_1^3 - 3x_1x_0^2}$$

$$b = \frac{3(K_0 - K_1)(x_0 + x_1)}{x_0^3 + 3x_0x_1^2 - x_1^3 - 3x_1x_0^2}$$

$$c = -6\frac{(K_0 - K_1)x_1x_0}{x_0^3 + 3x_0x_1^2 - x_1^3 - 3x_1x_0^2}$$

$$d = \frac{-x_1^3K_0 + 3x_1^2K_0x_0 + K_1x_0^3 - 3K_1x_1x_0^2}{x_0^3 + 3x_0x_1^2 - x_1^3 - 3x_1x_0^2}.$$

– The analytical solution is

$$u(x,t,\xi) = \begin{cases} K_0 & \text{si} \quad (x - \sigma\xi) - K_0 t < x_0 \\ aX^3(x,\xi) + bX^2(x,\xi) + cX(x,\xi) + d & \text{if} \quad x_0 \leqslant X(x,\xi) \leqslant x_1 \\ K_1 & \text{if} \quad X(x,\xi) \geqslant x_1 \end{cases}$$

where

$$X(x,\xi) = h(x - \sigma\xi) - \frac{a(3ct+3) - b^2}{9a^2 th} - \frac{b}{3a}$$

with

$$h(x) = \left(\left(\left(27a^2tx^2 + x(27a^2d^2 + (4b^3 - 18abc)d + 4ac^3 - b^2c^2)t^3((-54a^2d + 18abc - 4b^3)t^2 + 18abt) \right. \right. \right.$$

$$\left. \left. + (-18abd + 12ac^2 - 2b^2c)t^2 + (12ac - b^2)t + 4a)^{\frac{1}{2}} \right) \middle/ \left(6\sqrt{3}a^2t^{\frac{3}{2}}\right) - \frac{a^2(27dt - 27x) + ab(-9ct - 9) + 2b^3t}{54a^3t} \right)^{\frac{1}{3}}.$$
$$\tag{A.2}$$

In practice, we take $L = 3, K_0 = 12, K_1 = 1, x_0 = 0.5, x_1 = 1.5$ and $\sigma = 0.2$ so that $\sigma\xi \in [-0.2, 0.2]$.

A.3. 2D test-case IC_3

– Let the initial condition be $u^{IC_3} : (x, \xi_0, \xi_1) \in \mathcal{D} = [0,L] \times [-1,1] \times [-1,1] \rightarrow$, such that

$$u^{IC_4}(x, \xi_0, \xi_1) = (\overline{K_0} + \sigma_0\xi_0) \cdot {}_{[0,x_0]}(x) + (\overline{K_1} + \sigma_1\xi_1) \cdot {}_{[x_0,x_1]}(x) + K_2 \cdot {}_{[x_1,L]}(x)$$

with $\overline{K_0} + \sigma_0\xi_0 > \overline{K_1} + \sigma_1\xi_1 \forall (\xi_0, \xi_1) \in [-1,1] \times [-1,1]$ so that the solution for $0 < t < t^*$ is a succession of two shocks with the first one going faster than the second one.

– For $t > t^*$, the solution will result in only one shock propagating at the velocity $v^*(\xi_0) = \frac{K_0 + K_2}{2} = \frac{\overline{K_0} + \sigma_0\xi_0 + K_2}{2}$.

– Let's find out how t^* depends on (ξ_0, ξ_1). We denote by $v_0(\xi_0, \xi_1) = \frac{\overline{K_0} + \overline{K_1} + \sigma_0\xi_0 + \sigma_1\xi_1}{2}$ and $v_1(\xi_1) = \frac{\overline{K_1} + \sigma_1\xi_1 + K_2}{2}$ the velocities of the two shocks and by $x_0(t, \xi_0, \xi_1) = v_0(\xi_0, \xi_1)t + x_0^0$ and $x_1(t, \xi_1) = v_1(\xi_1)t + x_1^0$ their respective positions at an instant t. Then t^* is by definition the time where $x_0(t, \xi_0, \xi_1) = x_1(t, \xi_0, \xi_1)$. We have

$$t^*(\xi_0) = 2\frac{x_0^0 - x_1^0}{K_2 - \overline{K_0} - \sigma_0\xi_0} \quad \text{and} \quad x^*(\xi_0, \xi_1) = (x_0^0 - x_1^0)\frac{\overline{K_1} + \sigma_1\xi_1 + K_2}{K_2 - \overline{K_0} - \sigma_0\xi_0} + x_1^0. \tag{A.3}$$

  – In practice, we take $L = 1, \overline{K_0} = 12, \overline{K_1}6 = 6, K_2 = 1, x_0 = 0.3, x_1 = 0.6$ and $\sigma_0 = 0.2, \sigma_1 = 0.1$.

Appendix B. Upwinded Roe scheme for Burgers' equation

One particularity of our Burgers' test cases is that they are such that the eigenvalues of the P-truncated system are all positive ($\forall P$). Indeed, in the formalism of IPMM, for continuous solutions, (23) can be rewritten $\mathbb{A}\partial_t V + \quad \partial_x V = 0$ where $V = (v_0, \ldots, v_P)^t$,

$$\mathbb{A} = \int \begin{pmatrix} \nabla_v u\phi_0\phi_0 & \ldots & \nabla_v u\phi_0\phi_P \\ \ldots & \nabla_v u\phi_i\phi_j & \ldots \\ \nabla_v u\phi_P\phi_0 & \ldots & \nabla_v u\phi_P\phi_P \end{pmatrix} dw \quad \text{and} \quad = \int \begin{pmatrix} u\nabla_v u\phi_0\phi_0 & \ldots & u\nabla_v u\phi_0\phi_P \\ \ldots & u\nabla_v u\phi_i\phi_j & \ldots \\ u\nabla_v u\phi_P\phi_0 & \ldots & u\nabla_v u\phi_P\phi_P \end{pmatrix} dw.$$

If we denote by $(\lambda_k^P)_{k\in\{0,\ldots,P\}}$ the eigenvalues of Eq. (23) then we know that

$$\min_{x\in{}^P-\{0\}} \frac{\langle x, \, x\rangle}{\langle x, \mathbb{A}x\rangle} \leqslant \lambda_k^P \forall k \in \{0, \ldots, P\}.$$

We have $\langle x, \mathbb{A}x\rangle = \int \nabla_v u \times \left(\sum_{k=0}^P x_k\phi_k\right)^2 dw = \int \nabla_{vv}^2 s^* \times \left(\sum_{k=0}^P x_k\phi_k\right)^2 dw > 0$ as s^* is entropy (see Property 2.3.2). Besides $\langle x, \, x\rangle = \int u\nabla_v u \times \left(\sum_{k=0}^P x_k\phi_k\right)^2 dw \geqslant \int \min(u^0)\nabla_{vv}^2 s^* \times \left(\sum_{k=0}^P x_k\phi_k\right)^2 dw > 0$ as $\min(u^0) = \min_{(x,\xi)\in\mathcal{D}\times[-1,1]} u(x,0,\xi) > 0$ for the test cases we consider. Consequently, $0 \leqslant \lambda_k^P \forall k \in \{0, \ldots, P\}$. This inequality is independent of the choice of the entropy: it is valid for sG-gPC $\left(s(u) = \frac{u^2}{2}\right)$ and IPMM (general choice of s). In term of a Roe scheme, it means that if we have a Roe matrix $A(U)$ for Eq. (23), we have $|A(U)| = A(U)$ and the numerical flux expression is

$$F_{j+1/2}^n = \frac{1}{2}(F(U_j^n) + F(U_{j+1}^n)) - \frac{1}{2}|A(U_j^n, U_{j+1}^n)|(-U_j^n + U_{j+1}^n),$$

$$F_{j+1/2}^n = \frac{1}{2}(F(U_j^n) + F(U_{j+1}^n)) - \frac{1}{2}A(U_j^n, U_{j+1}^n)(-U_j^n + U_{j+1}^n),$$

$$\text{with } F(U) - F(V) = A(U, V)(U - V),$$

$$F_{j+1/2}^n = F(U_j^n) : \text{the flux is upwinded}.$$

Consequently, the same numerical scheme can be used to solve IPMM and sG-gPC for the problem considered: the computational cost and the numerical accuracy of both methods are comparable.

References

[1] R. Abgrall, A simple, flexible and generic deterministic approach to uncertainty quantifications in non linear problems: application to fluid flow problems, Rapport de Recherche INRIA (2007).
[2] S. Acharjee, N. Zabaras, Uncertainty propagation in finite deformations – A spectral stochastic Lagrangian approach, Comput. Methods Appl. Mech. Eng. 195 (2006) 2289–2312.
[3] R. Askey, J. Wilson, Some basic hypergeometric polynomials that generalize Jacobi polynomials, Memoirs Am. Math. Soc., AMS, Providence RI 319 (1985).
[4] G.K. Batchelor, The Theory of Homogeneous Turbulence, Cambridge University Press, Cambridge, 1953.
[5] J.B. Bell, J. Foo, A.L. Garcia, Algorithm refinement for the stochastic Burgers' equation, J. Comput. Phys. 223 (2007) 451–468.
[6] R.H. Cameron, W.T. Martin, The orthogonal development of non-linear functionals in series of fourier-hermite functionals, Ann. Math. 48 (1947) 385–392.
[7] G. Chen, C. Levermore, T. Liu, Hyperbolic Conservation Laws with Stiff Relaxation Terms and Entropy, 1994.
[8] Q.Y. Chen, D. Gottlieb, J.S. Hesthaven, Uncertainty analysis for the steady-state flows in a dual throat nozzle, J. Comput. Phys. 204 (2005) 78–398.
[9] A.J. Chorin, Gaussian fields and random flow, J. Fluid. Mech. 63 (1974) 21–32.
[10] B. Ganapathysubramanian, N. Zabaras, Sparse grid collocation schemes for stochastic natural convection problems, J. Comput. Phys. 225 (2007) 652–685.
[11] R.G. Ghanem, P. Spanos, Stochastic Finite Elements: A Spectral Approach, Springer-Verlag, 1991.
[12] E. Godlevski, P.A. Raviart, Hyperbolic Systems of Conservation Laws, Ellipse, Paris, 1991.
[13] M. Griebel, H.-J. Bungartz, Sparse grids, Acta Numer. (2004) 1–123.
[14] T.Y. Hou, B. Rozovskii, W. Luo, H.-M. Zhou, Wiener Chaos expansions and numerical solutions of randomly forced equations of fluid mechanics, J. Comput. Phys. 216 (2006) 687–706.
[15] J. Jourdren, S. Del Pino, Arbitrary high-order schemes for the linear advection and wave equations: application to hydrodynamics and aeroacoustics, C.R. Acad. Sci. Paris, Ser. I 342 (2006) 441–446.
[16] J. Ko, D. Lucor, P. Sagaut, Sensitivity of two dimensional spatially developing mixing layers with respect to uncertain inflow conditions, Phys. Fluids 20 (7) (2008) 077102.
[17] R. Koekoek, R.F. Swarttouw, The Askey-scheme of hypergeometric orthogonal polynomials and its q-analogue, Technical Report 98-17, Department of Technical Mathematics and Informatics, Delft University of Technology, 1998.
[18] O. Le Maitre, M. Reagan, H. Najm, R. Ghanem, O. Knio, Multi-resolution analysis of Wiener-type uncertainty propagation schemes, J. Comput. Phys. 197 (2004) 502–531.

[19] G. Lin, C.-H. Su, G.E. Karniadakis, The stochastic piston problem, PNAS 101 (45) (2004) 15840–15845.
[20] G. Lin, C.-H. Su, G.E. Karniadakis, Stochastic solvers for the euler equations, 43rd AIAA Aerospace Sci. Meet. Exhibit (0873) (2005) 10–13.
[21] G. Lin, C.-H. Su, G.E. Karniadakis, Predicting shock dynamics in the presence of uncertainties, J. Comp. Phys. (217) (2006) 260–276.
[22] G. Lin, C.-H. Su, G.E. Karniadakis, Stochastic modeling of random roughness in shock scattering problems: theory and simulations, Comput. Methods Appl. Mech. Eng., doi:10.1016/j.cma.2008.02.025.
[23] D. Lucor, C. Enaux, H. Jourdren, P. Sagaut, Multi-physics stochastic design optimization: application to reacting flows and detonation, Comput. Methods Appl. Mech. Eng. 196 (2007) 5047–5062.
[24] D. Lucor, G.E. Karniadakis, Noisy inflows cause a shedding-mode switching in flow past an oscillating cylinder, Phys. Rev. Lett. 92 (15) (2004) 154501-1–154501-4.
[25] D. Lucor, J. Meyers, P. Sagaut, Sensitivity analysis of LES to subgrid-scale-model parametric uncertainty using Polynomial Chaos, J. Fluid Mech. 585 (2007) 255–279.
[26] O.P. Le Maître, O.M. Knio, Uncertainty propagation using Wiener–Haar expansions, J. Comput. Phys. 197 (2004) 28–57.
[27] O.P. Le Maître, O.M. Knio, A stochastic particle-mesh scheme for uncertainty propagation in vortical flows, J. Comput. Phys. 226 (2007) 645–671.
[28] L. Mathelin, O. P. Le Maître, A posteriori error analysis for stochastic finite element solutions of fluid flows with parametric uncertainties, in: European Conference on Computational Fluid Dynamics, ECCOMAS CFD, 2006.
[29] H. Matthies, A. Keese, Galerkin methods for linear and nonlinear elliptic stochastic partial differential equations, Comput. Methods Appl. Mech. Eng. 192 (12–16) (2005) 1295–1331.
[30] I. Müller, T. Ruggeri, Rational Extended Thermodynamics, second ed., Springer; I. Müller, T. Ruggeri, Tracts in Natural Philosophy, vol. 37, Springer-Verlag, New York, 1998.
[31] H. Ogura, Orthogonal functionals of the Poisson process, IEEE Trans. Info. Theory IT-18 (1972) 473–481.
[32] H.N. Najm, O.P. Le Maître, O.M. Knio, R.G. Ghanem, A stochastic projection method for fluid flow I: basic formulation, J. Comput. Phys. 173 (2001) 481–511.
[33] W. Schoutens, Stochastic Processes and Orthogonal Polynomials, Springer-Verlag, New York, 2000.
[34] D. Serre, Systèmes hyperboliques de lois de conservation, parties I et II, Diderot, Paris, 1996.
[35] P. Spanos, R.G. Ghanem, Stochastic finite element expansion for random media, ASCE J. Eng. Mech. 115 (5) (1989) 1035–1053.
[36] G. Szego, Orthogonal Polynomials, vol. 23, Am. Math. Soc., Colloquim Publications, 1939.
[37] E.F. Toro, Riemann Solver and Numerical Methods for Fluid Dynamics, Springer-Verlag, 1997.
[38] E. Novak, V. Barthelmann, K. Ritter, High dimensional polynomial interpolation on sparse grids, Mathematics Subject Classification (1991).
[39] X. Wan, G.E. Karniadakis, Stochastic heat transfer enhancement in a grooved channel, J. Fluid Mech. 565 (2006) 255–278.
[40] X. Wan, G.E. Karniadakis, Long-term behavior of Polynomial Chaos in stochastic flow simulations, Comput. Methods Appl. Mech. Eng. 195 (2006) 5582–5596.
[41] X. Wan, G.E. Karniadakis, Multi-Element generalized Polynomial Chaos for arbitrary probability measures, SIAM J. Sci. Comput. 28 (3) (2006) 901–928.
[42] N. Wiener, The homogeneous chaos, Am. J. Math. 60 (1938) 897–936.
[43] D. Xiu, G.E. Karniadakis, The Wiener–Askey Polynomial Chaos for stochastic differential equations, SIAM J. Sci. Comput. 24 (2) (2002) 619–644.
[44] D. Xiu, D. Lucor, G.E. Karniadakis, Stochastic modeling of flow-structure interactions, in: K.J. Bathe (Ed.), Computational Fluid and Solid Mechanics, Proceedings of the 1st MIT Conference, vol. 2, Elsevier, Cambridge, Massachussetts, 2001, pp. 1420–1423.
[45] D. Xiu, D. Lucor, C.-H. Su, G.E. Karniadakis, Stochastic modeling of flow-structure interactions using generalized Polynomial Chaos, J. Fluid Eng. 124 (2002) 51–59.